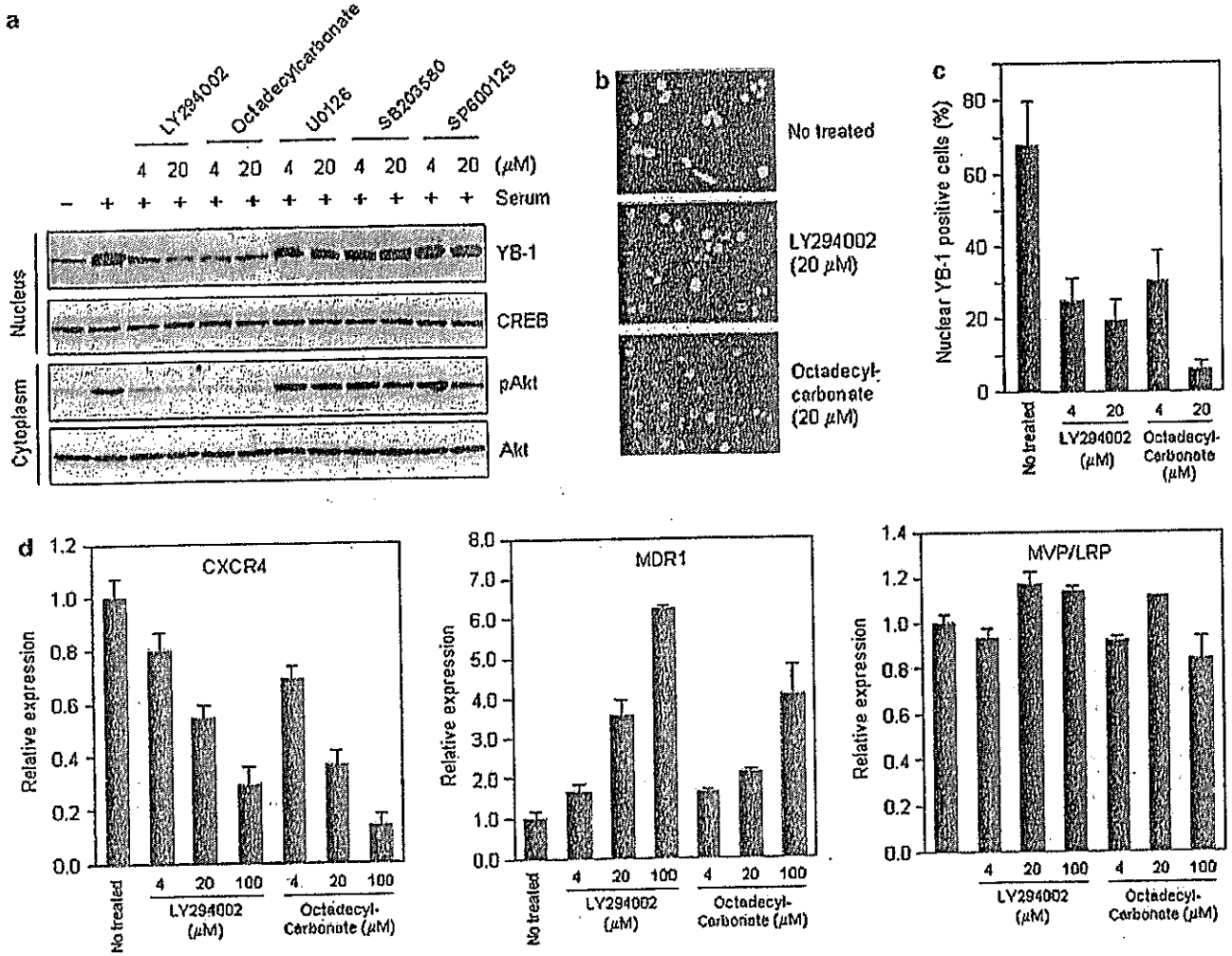

Figure 5 Akt activity is required for YB-1 nuclear accumulation and transcriptional regulation by YB-1. (a) The effect of kinase inhibitors on the nuclear accumulation of YB-1 in SKOV-3 cells. Inhibitors were added 3 h before serum stimulation and nuclear extracts were prepared 1 h after serum stimulation. Anti-YB-1 and anti-CREB immunoblots were performed with nuclear extracts, and anti-pAkt and anti-Akt immunoblots were performed on cytoplasmic extracts. CREB and Akt are shown as a loading control. (b) Immunofluorescent staining for YB-1. SKOV-3 cells were treated with LY294002 or octadecylcarbonate for 24 h and then stained with YB-1. Cells were fixed and permeabilized, incubated at 4°C with the primary YB-1 antibody, then with the Alexa Flour 546-labelled secondary antibody. (c) Quantitative analysis of YB-1 nuclear localization in SKOV-3 cells as shown in Figure 2b. Data are mean of three independent experiments; bars ±s.d. (d) QRT-PCR for MDR1, MVP/LRP, CXCR4 and housekeeping gene GAPDH. The relative gene expression for each sample was determined using the formula $2^{(-\Delta C_t)} = 2^{(C_t(\mathrm{GAPDH}) - C_t(\mathrm{target}))}$ which reflected target gene expression normalized to GAPDH levels. Data were mean of three independent experiments; bars ±s.d.

the development of tumor growth, angiogenesis and metastasis not only in ovarian cancer (Scotton *et al.*, 2002) but also in other tumor types including breast cancer (Muller *et al.*, 2001), melanoma (Robledo *et al.*, 2001; Murakami *et al.*, 2004), and prostate cancer (Darash-Yahana *et al.*, 2004). Jiang *et al.* (2006) further demonstrated that CXCR4 expression could be an important prognostic marker for ovarian cancers: the rate of CXCR4 expression in refractory and recurrent group was significantly higher than that in non-recurrent group. Our previous studies showed a significant association of nuclear localization of YB-1 with unfavorable prognosis of patients with ovarian cancers (Kamura *et al.*, 1999; Huang *et al.*, 2004). Clinicopathological analysis whether nuclear expression of YB-1 can be associated with CXCR4 expression or CXCL12 (SDF-1α) in patients with ovarian cancers is now in progress.

Several studies have focused on the role of Akt/PI3K inhibitors as potential tumor suppressor agents. It has been reported that phosphorylation of Akt and mTOR, an Akt substrate, was frequently detected in ovarian cancer (Altomare *et al.*, 2004). In animal model of ovarian cancer, LY294002, a potent inhibitor of Akt activation, could inhibit cancer growth and ascites formation (Hu *et al.*, 2000). Our study also

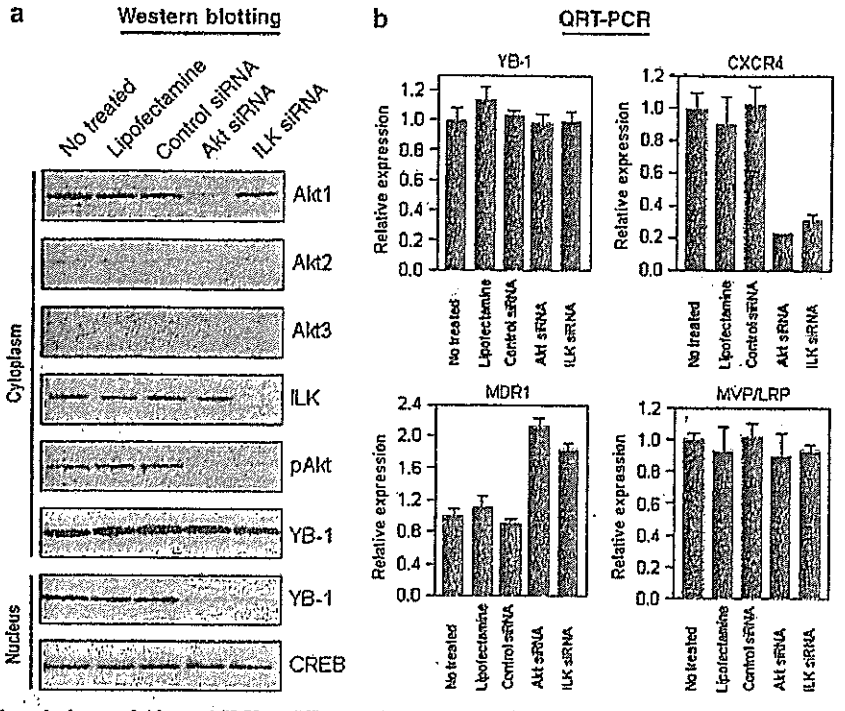

Figure 6 Effect of knock down of Akt and ILK on YB-1 nuclear accumulation, and expression of MDR1, MVP/LRP and CXCR4. (a) SKOV-3 cells were treated with Akt siRNA (100 nM), ILK siRNA (10 nM) or control siRNA (100 nM) for 48 h, and then cytoplasmic and nuclear extracts were prepared. Anti-Akt1, anti-Akt2, anti-Akt3, anti-ILK, anti-pAkt, and anti-YB-1 immunoblots were performed with cytoplasmic extracts, and anti-YB-1 and anti-CREB immunoblots were performed with nuclear extracts. (b) SKOV-3 cells were treated with Akt siRNA (100 nM) or ILK siRNA (10 nM) for 48 h and then total RNA was prepared. QRT-PCR was performed for MDR1, MVP/LRP, CXCR4, YB-1 and GAPDH housekeeping gene. The relative gene expression for each sample was determined using the formula $2^{(-\Delta C_t)} = 2^{(C_t(\text{GAPDH}) - C_t(\text{target}))}$ which reflected target genes normalized to GAPDH levels. Data were mean of three independent experiments; bars ±s.d.

demonstrated that both Akt phosphorylation and YB-1 nuclear localization were blocked by administration of LY294002 in SKOV-3 xenograft model. Nuclear localization of YB-1 is induced through various pathways including Akt (see Introduction). The Akt-dependent pathway for YB-1 nuclear localization would provide further insight how Akt-targeting anticancer therapeutic strategy could be developed.

In conclusion, we have identified several genes that are regulated by YB-1 and/or its nuclear localization. Further immunohistochemical analysis should be required to elucidate the role of YB-1 in the expression of *CXCR4* and other relevant genes that are associated with the clinicopathological characteristics in human ovarian cancers. Based on our present experimental results, we aim to present YB-1 and YB-1-dependent gene networks as molecular targets for the further development of novel anticancer therapeutic strategies.

Materials and methods

Cell culture and reagents

OVCAR-3 and SKOV-3 were purchased from American Type Culture Collection (Manassas, VA, USA). RMG-I, RMG-II, RMG-III, RMBG and RTSG were kindly provided by Dr S Nozawa, Department of Obstetrics and Gynecology, Keio University. These cell lines were grown in DMEM supplemented with 10% fetal bovine serum (FBS) in an atmosphere of 5% CO_2. LY294002 and U0126 were purchased from Sigma Chemical Co. (St Louis, MO, USA). 1L-6-hydroxymethyl-*chiro*-inositol 2(*R*)-2-*O*-methyl-3-*O*-octadecylcarbonate (Hu *et al*., 2000), SB203580 (Cuenda *et al*., 1995), and SP600125 (Bennett *et al*., 2001) were obtained from Calbiochem (San Diego, CA, USA). Anti-YB-1 was generated as described previously (Ohga *et al*., 1996). Anti-CREB, anti-PKB/Akt, anti-phospho-PKB/Akt, anti-ILK, Akt siRNA and ILK siRNA were obtained from Cell Signaling Technology (Beverly, MA, USA).

Western blotting

Western blotting was performed as previously described (Kaneko *et al*., 2004). Cells were lysed in buffer A (10 mM HEPES (pH7.9), 10 mM KCl, 10 mM EDTA, 1 mM DTT, 0.4% v/v IGEPAL, 1 mM Na_3VO_4, 1 mM PMSF, and 10 μg/ml aprotinin and leupeptin) for 10 min on ice, and then centrifuged for 3 min at 15 000 r.p.m. The supernatant fractions (cytoplasmic soluble proteins) were collected. The nuclear pellet was then washed and then lysed in buffer C (20 mM HEPES (pH7.9), 200 mM NaCl, 1 mM EDTA, 5% v/v glycerol, 1 mM DTT, 1 mM Na_3VO_4, 1 mM PMSF and 10 μg/ml aprotinin and leupeptin). Lysates were incubated on ice for 2 h, and then centrifuged 15 000 r.p.m. for 5 min. The lysates were separated by sodium dodecyl sulfate–polyacryl amide gel electrophoresis (SDS–PAGE), and then were transferred to a nitrocellulose membrane. The membrane were incubated with the primary antibody and visualized with secondary antibody coupled to horseradish peroxidase (Cell Signaling Technology)

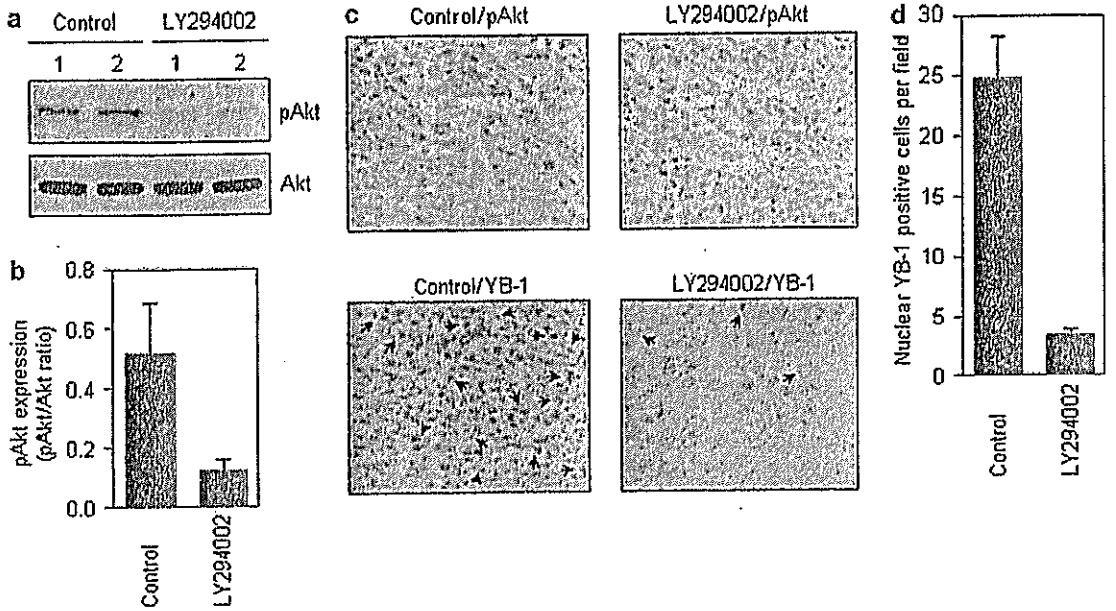

Figure 7 Effect of LY294002 on Akt phosphorylation and YB-1 nuclear localization in SKOV-3 xenograft. (a) Effect of LY294002 on Akt phosphorylation in SKOV-3 xenograft. SKOV-3 cells were injected subcutaneously (5.0×10^6 cells/0.1 ml/mouse). When tumors reached approximately 1000–2000 mm^3, animals were randomly assigned to two groups of five. The first group received i.p. injections of DMSO as a control. The second group received i.p. injections of 50 mg/kg LY294002. One hour after LY294002 injection, mice were killed humanely (while anesthetized) by cervical dislocation and tumors were excised. Western blot analysis was carried out using cytosolic extracts prepared from tumor tissues from two animals treated with or without drug. (b) Quantitative analysis of Akt phosphorylation in SKOV-3 tumor xenograft. Levels of Akt phosphorylation were normalized to their nonphosphorylated form as shown in Figure 7a. Data are expressed as mean ± s.d. of three to five mice. (c) Immunohistochemical staining was carried out using conventional protocols. The arrows indicate positive cell nuclei staining for YB-1 (×200 magnification). (d) Quantitative analysis of YB-1 nuclear localization in SKOV-3 tumor xenograft. YB-1 nuclear localization was determined by counting the number of positive YB-1 nuclear cells in high-power fields as shown in Figure 7b. Data were mean of each section (five sections per mouse). Columns, mean; bars ± s.d.

and SuperSignal West Pico Chemiluminescent Substrate (Pierce, Rockford, IL, USA). Bands on Western blots were analysed densitometrically using Scion Image software (version 4.0.2; Scion Corp., Frederick, MD, USA).

Oligonucleotide microarray analysis

The siRNA corresponding to nucleotide sequences of the YB-1 (5′-GGU UCC CAC CUU ACU ACA U-3′) was purchased from QIAGEN Inc. (Valencia, CA, USA). A negative control siRNA was obtained from Invitrogen (Carlsbad, CA, USA). siRNA duplexes were transfected using LipofectAMINE2000 and Opti-MEM medium (Invitrogen) according to the manufacturer's recommendations. Duplicate samples were prepared for microarray hybridization. At 48 h after siRNA transfection, total RNA was extracted from cell cultures using ISOGEN (Nippon Gene Co. Ltd., Tokyo, Japan). Total RNA (2 μg) was reverse-transcribed using GeneChip 3′-Amplification Reagents One-Cycle cDNA Synthesis Kit (Affymetrix Inc., Santa Clara, CA, USA) and then labeled with Cy5 or Cy3. The labeled cRNA was applied to the oligonucleotide microarray (Human Genome U133 Plus 2.0 Array, Affymetrix). The microarray was scanned on a GeneChip Scanner3000 and the image was analysed using a GeneChip Operating Software ver1.

Correlation analysis of gene expression, and clustering of cell lines and genes expression

Gene expression data for the 60 human tumor cell lines were obtained from the Developmental Therapeutics Program (http://www.dtp. nci.nih.gov/), expressed as log of the mRNA levels in cell line/mRNA levels in reference pool in the NCI screen. Pearson correlation coefficients were calculated for each gene–gene pair. Hierarchical clustering can be used to group cell lines and genes in term of their patterns of gene expression. To obtain cluster trees for genes that showed distinct expression patterns across the 60 cell lines, we used the program 'Cluster' and 'Tree View' (http://rana.lbl.gov/) with average linkage clustering and a correlation metric (Eisen *et al.*, 1998).

Quantitative real-time polymerase chain reaction

RNA was reverse transcribed from random hexamers using AMV reverse transcriptase (Promega, Madison, WI, USA). Real-time quantitative PCR was performed using the Real-Time PCR system 7300 (Applied Biosystems, Foster City, CA, USA) as described previously (Maruyama *et al.*, 2006). In brief, the PCR amplification reaction mixtures (20 μl) contained cDNA, primer pairs, the dual-labeled fluorogenic probe, and TaqMan Universal PCR Master Mix (Applied Biosystems). The thermal cycle conditions included maintaining the reactions at 50°C for 2 min and at 95°C for 10 min, and then alternating for 40 cycles between 95°C for 15 s and 60°C for 1 min. The primer pairs and the probe were obtained from Applied Biosystems. The relative gene expression for each sample was determined using the formula $2^{(-\Delta C_t)} = 2^{(C_t(\mathrm{GAPDH}) - C_t(\mathrm{target}))}$ which reflected target gene expression normalized to GAPDH levels.

Immunofluorescence

Cells were plated on glass coverslips in six-well plates and allowed to attach overnight. Then, cells were rinsed with PBS

and then fixed in 4% paraformaldehyde/PBS for 30 min. Cells were rinsed twice with PBS and then permeabilized with 0.5 ml of solution containing 5% BSA, 0.2% Triton X-100 in PBS for 90 min. After 1 h of blocking with 2% goat serum, the cells were incubated overnight with primary antibody at 4°C in 1% BSA in PBS. Cells were then rinsed three times with PBS and incubated with 1 μg/ml of Alexa Flour 546-labeled secondary antibody (Molecular Probe, Eugene, OR, USA) in 1% BSA in PBS for 60 min. Coverslips were mounted on slide glasses using gel mount and viewed using an Olympus BX51 florescence microscope (Tokyo, Japan) and photographed with Olympus DP-70 digital camera.

Tumor xenograft study

Male BALB/c nude mice were obtained from Kyudo Co., Ltd. (Fukuoka, Japan). SKOV-3 cells were harvested and resuspended in PBS. The suspension was injected subcutaneously in the mice (5.0×10^6 cells/0.1 ml/mouse). When tumors reached about 1000–2000 mm^3, animals were randomly assigned to two groups of five mice each. The first group received i.p. injections of DMSO as control. The second group received i.p. injection of LY294002 at 50 mg/kg. At 1 h after LY294002 injection, mice were killed humanly (mice still anesthetized) by cervical dislocation and tumors were excised. For immunohistchemistry, one part of the tumor tissue was fixed in formalin and embed in paraffin.

Acknowledgements

We thank Y Yamada and Y Yamasaki in Hanno Research Center of Taiho Pharmaceutical Co. Ltd. for fruitful discussion, and N Shinbaru in Kyushu University for editorial help. This study was supported by the COE program for Medical Sciences, Kurume University, and grant-in-aid for scientific research on priority areas cancer from Ministry of Education Culture, Sports Science, and Technology of Japan and the 2nd-Comprehensive Ten-Year Strategy for Cancer Control from the Ministry of Health, Welfare and Labor, Japan.

References

Altomare DA, Wang HQ, Skele KL, De Rienzo A, Klein-Szanto AJ, Godwin AK *et al.* (2004). AKT and mTOR phosphorylation is frequently detected in ovarian cancer and can be targeted to disrupt ovarian tumor cell growth. *Oncogene* **23**: 5853–5857.

Asakuno K, Kohno K, Uchiumi T, Kubo T, Sato S, Isono M *et al.* (1994). Involvement of a DNA binding protein, MDR-NF1/YB-1, in human MDR1 gene expression by actinomycin D. *Biochem Biophys Res Commun* **199**: 1428–1435.

Ashizuka M, Fukuda T, Nakamura T, Shirasuna K, Iwai K, Izumi H *et al.* (2002). Novel translational control through an iron-responsive element by interaction of multifunctional protein YB-1 and IRP2. *Mol Cell Biol* **22**: 6375–6383.

Bargou RC, Jurchott K, Wagener C, Bergmann S, Metzner S, Bommert K *et al.* (1997). Nuclear localization and increased levels of transcription factor YB-1 in primary human breast cancers are associated with intrinsic MDR1 gene expression. *Nat Med* **3**: 447–450.

Bennett BL, Sasaki DT, Murray BW, O'Leary EC, Sakata ST, Xu W *et al.* (2001). SP600125, an anthrapyrazolone inhibitor of Jun N-terminal kinase. *Proc Natl Acad Sci USA* **98**: 13681–13686.

Caruz A, Samsom M, Alonso JM, Alcami J, Baleux F, Virelizier JL *et al.* (1998). Genomic organization and promoter characterization of human CXCR4 gene. *FEBS Lett* **426**: 271–278.

Cuenda A, Rouse J, Doza YN, Meier R, Cohen P, Gallagher TF *et al.* (1995). SB 203580 is a specific inhibitor of a MAP kinase homologue which is stimulated by cellular stresses and interleukin-1. *FEBS Lett* **364**: 229–233.

Darash-Yahana M, Pikarsky E, Abramovitch R, Zeira E, Pal B, Karplus R *et al.* (2004). Role of high expression levels of CXCR4 in tumor growth, vascularization, and metastasis. *FASEB J* **18**: 1240–1242.

Dooley S, Said HM, Gressner AM, Floege J, En-Nia A, Mertens PR. (2006). Y-box protein-1 is the crucial mediator of antifibrotic interferon-gamma effects. *J Biol Chem* **281**: 1784–1795.

Eisen MB, Spellman PT, Brown PO, Botstein D. (1998). Cluster analysis and display of genome-wide expression patterns. *Proc Natl Acad Sci USA* **95**: 14863–14868.

En-Nia A, Yilmaz E, Klinge U, Lovett DH, Stefanidis I, Mertens PR. (2005). Transcription factor YB-1 mediates DNA polymerase alpha gene expression. *J Biol Chem* **280**: 702–711.

Evdokimova V, Ruzanov P, Imataka H, Raught B, Svitkin Y, Ovchinnikov LP *et al.* (2001). The major mRNA-associated protein YB-1 is a potent 5′ cap-dependent mRNA stabilizer. *EMBO J* **20**: 5491–5502.

Fukuda T, Ashizuka M, Nakamura T, Shibahara K, Maeda K, Izumi H *et al.* (2004). Characterization of the 5′-untranslated region of YB-1 mRNA and autoregulation of translation by YB-1 protein. *Nucleic Acids Res* **32**: 611–622.

Furukawa M, Uchiumi T, Nomoto M, Takano H, Morimoto RI, Naito S *et al.* (1998). The role of an inverted CCAAT element in transcriptional activation of the human DNA topoisomerase IIalpha gene by heat shock. *J Biol Chem* **273**: 10550–10555.

Holm PS, Bergmann S, Jurchott K, Lage H, Brand K, Ladhoff A *et al.* (2002). YB-1 relocates to the nucleus in adenovirus-infected cells and facilitates viral replication by inducing E2 gene expression through the E2 late promoter. *J Biol Chem* **277**: 10427–10434.

Hu L, Zaloudek C, Mills GB, Gray J, Jaffe RB. (2000). *In vivo* and *in vitro* ovarian carcinoma growth inhibition by a phosphatidylinositol 3-kinase inhibitor (LY294002). *Clin Cancer Res* **6**: 880–886.

Huang X, Ushijima K, Komai K, Takemoto Y, Motoshima S, Kamura T *et al.* (2004). Co-expression of Y box-binding protein-1 and P-glycoprotein as a prognostic marker for survival in epithelial ovarian cancer. *Gynecol Oncol* **93**: 287–291.

Ise T, Nagatani G, Imamura T, Kato K, Takano H, Nomoto M *et al.* (1999). Transcription factor Y-box binding protein 1 binds preferentially to cisplatin-modified DNA and interacts with proliferating cell nuclear antigen. *Cancer Res* **59**: 342–346.

Jiang YP, Wu XH, Shi B, Wu WX, Yin GR. (2006). Expression of chemokine CXCL12 and its receptor CXCR4 in human epithelial ovarian cancer: an independent prognostic factor for tumor progression. *Gynecol Oncol* **103**: 226–233.

Kamura T, Yahata H, Amada S, Ogawa S, Sonoda T, Kobayashi H *et al.* (1999). Is nuclear expression of Y box-binding protein-1 a new prognostic factor in ovarian serous adenocarcinoma? *Cancer* **85**: 2450–2454.

Kaneko Y, Kitazato K, Basaki Y. (2004). Integrin-linked kinase regulates vascular morphogenesis induced by vascular endothelial growth factor. *J Cell Sci* **117**: 407–415.

Kohno K, Izumi H, Uchiumi T, Ashizuka M, Kuwano M. (2003). The pleiotropic functions of the Y-box-binding protein, YB-1. *Bioessays* **25**: 691–698.

Koike K, Uchiumi T, Ohga T, Toh S, Wada M, Kohno K *et al.* (1997). Nuclear translocation of the Y-box binding protein by ultraviolet irradiation. *FEBS Lett* **417**: 390–394.

Kryczek I, Lange A, Mottram P, Alvarez X, Cheng P, Hogan M *et al.* (2005). CXCL12 and vascular endothelial growth factor synergistically induce neoangiogenesis in human ovarian cancers. *Cancer Res* **65**: 465–472.

Kuwano M, Oda Y, Izumi H, Yang SJ, Uchiumi T, Iwamoto Y *et al.* (2004). The role of nuclear Y-box binding protein 1 as a global marker in drug resistance. *Mol Cancer Ther* **3**: 1485–1492.

Ladomery M, Sommerville J. (1995). A role for Y-box proteins in cell proliferation. *Bioessays* **17**: 9–11.

Maruyama Y, Ono M, Kawahara A, Yokoyama T, Basaki Y, Kage M *et al.* (2006). Tumor growth suppression in pancreatic cancer by a putative metastasis suppressor gene Cap43/NDRG1/Drg-1 through modulation of angiogenesis. *Cancer Res* **66**: 6233–6242.

Matsumoto K, Wolffe AP. (1998). Gene regulation by Y-box proteins: coupling control of transcription and translation. *Trends Cell Biol* **8**: 318–323.

Mossink MH, van Zon A, Scheper RJ, Sonneveld P, Wiemer EA. (2003). Vaults: a ribonucleoprotein particle involved in drug resistance? *Oncogene* **22**: 7458–7467.

Muller A, Homey B, Soto H, Ge N, Catron D, Buchanan ME *et al.* (2001). Involvement of chemokine receptors in breast cancer metastasis. *Nature* **410**: 50–56.

Murakami T, Maki W, Cardones AR, Fang H, Tun Kyi A, Nestle FO *et al.* (2002). Expression of CXC chemokine receptor-4 enhances the pulmonary metastatic potential of murine B16 melanoma cells. *Cancer Res* **62**: 7328–7334.

Ohga T, Koike K, Ono M, Makino Y, Itagaki Y, Tanimoto M *et al.* (1996). Role of the human Y box-binding protein YB-1 in cellular sensitivity to the DNA-damaging agents cisplatin, mitomycin C, and ultraviolet light. *Cancer Res* **56**: 4224–4228.

Ohga T, Uchiumi T, Makino Y, Koike K, Wada M, Kuwano M *et al.* (1998). Direct involvement of the Y-box binding protein YB-1 in genotoxic stress-induced activation of the human multidrug resistance 1 gene. *J Biol Chem* **273**: 5997–6000.

Porcile C, Bajetto A, Barbieri F, Barbero S, Bonavia R, Biglieri M *et al.* (2005). Stromal cell-derived factor-1alpha (SDF-1alpha/CXCL12) stimulates ovarian cancer cell growth through the EGF receptor transactivation. *Exp Cell Res* **308**: 241–253.

Robledo MM, Bartolome RA, Longo N, Rodriguez-Frade JM, Mellado M, Longo I *et al.* (2001). Expression of functional chemokine receptors CXCR3 and CXCR4 on human melanoma cells. *J Biol Chem* **276**: 45098–45105.

Scotton CJ, Wilson JL, Milliken D, Stamp G, Balkwill FR. (2001). Epithelial cancer cell migration: a role for chemokine receptors? *Cancer Res* **61**: 4961–4965.

Scotton CJ, Wilson JL, Scott K, Stamp G, Wilbanks GD, Fricker S *et al.* (2002). Multiple actions of the chemokine CXCL12 on epithelial tumor cells in human ovarian cancer. *Cancer Res* **62**: 5930–5938.

Sorokin AV, Selyutina AA, Skabkin MA, Guryanov SG, Nazimov IV, Richard C *et al.* (2005). Proteasome-mediated cleavage of the Y-box-binding protein 1 is linked to DNA-damage stress response. *EMBO J* **24**: 3602–3612.

Stein U, Bergmann S, Scheffer GL, Scheper RJ, Royer HD, Schlag PM *et al.* (2005). YB-1 facilitates basal and 5-fluorouracil-inducible expression of the human major vault protein (MVP) gene. *Oncogene* **24**: 3606–3618.

Stein U, Jurchott K, Walther W, Bergmann S, Schlag PM, Royer HD. (2001). Hyperthermia-induced nuclear translocation of transcription factor YB-1 leads to enhanced expression of multidrug resistance-related ABC transporters. *J Biol Chem* **276**: 28562–28569.

Stenina OI, Poptic EJ, DiCorleto PE. (2000). Thrombin activates a Y box-binding protein (DNA-binding protein B) in endothelial cells. *J Clin Invest* **106**: 579–587.

Sutherland BW, Kucab J, Wu J, Lee C, Cheang MC, Yorida E *et al.* (2005). Akt phosphorylates the Y-box binding protein 1 at Ser102 located in the cold shock domain and affects the anchorage-independent growth of breast cancer cells. *Oncogene* **24**: 4281–4292.

Supplementary Information accompanies the paper on the Oncogene website (http://www.nature.com/onc).

Cancer Chemother Pharmacol
DOI 10.1007/s00280-006-0314-6

EGFR mutation in various tissues

Kazuto Nishio · Tokuzo Arao · Terufumi Kato · Hideyuki Yokote

© Springer-Verlag 2006

Abstract Somatic mutations have been demonstrated in various tumors. *EGFR* mutations were first demonstrated in adenocarcinoma of the lung, and a large-scale retrospective study has clearly shown that these mutations are specifically observed in this form of the disease. Recently, possible occurrence of *EGFR* mutations in other tumor types including ovarian and colorectal malignancies has been reported. This raises the possibility of application of EGFR-specific tyrosine kinase inhibitors (EGFR-TKI) to the treatment of these malignancies, although broad success in this venture would depend on the frequency of such mutations. In this article, we discuss somatic mutations in various tumors as well as potential application of TKI to their treatment. Ethnic difference in the frequency of somatic mutations is another area of interest since it is closely related to clinical response to EGFR-TKIs. Preliminary studies have revealed such ethnic variations regarding *EGFR* mutation and gene amplification. Ethnic difference of transcriptional regulation of *EGFR* has also been demonstrated. We recently found a biomarker related to clinical response to EGFR-TKI that might explain the ethnic differences in response to this therapy. Various tyrosine kinases are known targets of TKIs. Thus genomics of individual patients may allow personalized target-based therapeutics.

Keywords EGFR mutation · Tyrosine kinase inhibitor · Ethnicity · HLA

This work was presented at the 21st Bristol-Myers Squibb Nagoya International Cancer Treatment Symposium, "Lung Cancer: Novel Therapy against Malfunctioning Molecules", 24–25 February 2006, Nagoya, Japan.

K. Nishio (✉) · T. Arao · T. Kato · H. Yokote
Pharmacology Division, National Cancer Center Research Institute, Tsukiji 5-1-1, Chuo-ku, Tokyo 104-0045, Japan
e-mail: knishio@med.kindai.ac.jp

K. Nishio · T. Arao · H. Yokote
Department of Genome Biology,
Kinki University School of Medicine, Osaka, Japan

EGFR mutation in various cancers

Somatic mutations have been demonstrated in various tumors. *EGFR* mutations were first demonstrated in adenocarcinoma of the lung, and a large-scale retrospective study has clearly shown that these mutations are specifically observed in this form of the disease [10]. However, extensive analysis of somatic mutation in various tumors subsequently demonstrated the existence of *EGFR* somatic mutation in many human tumors such as colorectal and head and neck cancer, renal cell carcinoma, prostate cancer, and cholangiocarcinoma [4, 7, 8]. Gwak et al. [5] reported *EGFR* mutation in cholangiocarcinoma and found that it was detectable in 13.6% (3/22) of patients. The type of mutation was deletion of exon 19. This is commonly observed in intrahepatic and poorly differentiated tumors. These and other researchers also reported this *EGFR* mutation in squamous cell head and neck carcinoma [7], and Cohen's group demonstrated a new mutation on *erb2* and gene amplification in this disease [3]. The mutation has also been reported in persistent ovarian and primary peritoneal carcinoma in clinical phase II trials of gefitinib [14]. Similar types of mutation have been reported in lung cancers, although these seem to be of minor occurrence [4]. Thus somatic mutations of *EGFR* exist in various tumors. Because of limited samples, it

remains unknown whether *EGFR* mutation in cancer is correlated with clinical response to EGFR-specific tyrosine kinase inhibitors (EGFR-TKI). *EGFR* mutation in other types of tumors than lung cancer seems correlated with immunohistochemical expression but correlation with gene amplification is unknown [14]. Functional aspects of *EGFR* mutation in other types of tumors are also only partially understood. To clarify the significance of somatic mutations in various tumors, tissue banking is necessary. In addition, validated and standardized analytical methods and cross-validation are important to give consistent results. We should also consider how to conduct clinical trials of target-based drugs for less common tumors based on biological data.

Ethnic difference in *EGFR* mutation

Ethnic difference in *EGFR* mutation is another important topic. It is considered that ethnic differences may determine both the frequency of *EGFR* mutation and response to TKi [2]. However, although it has not been fully discussed whether these differences are due to ethnic or merely geographical divides, ethnicity can explain differences in clinical response because of the data acquired in Asian–US patients. It is also considered that differences among the regions of Asia might be obtained: patterns of *EGFR* mutation may differ between Japanese, Chinese, Korean, South Indian, and Turkish individuals [16]. Expanding genome databases should eventually pinpoint the contribution of ethnicity in this regard. Already there is some evidence related to ethnic differences. A CA repeat exists in exon 1 of *EGFR*, related to transcriptional level of this gene. The length of CA repeat varies and is related to ethnicity [9]. Japanese have longer CA repeat compared with Caucasians. Moreover, intron 1 polymorphism reportedly mediates response to EGFR-TKI [1].

What are the differences among the types of *EGFR* mutation? The deletion mutation in exon 19 and point mutation L858R in exon 21 are the two major mutations. Previously, we speculated that the deletion mutation is more frequently detected in Japanese and Asian lung cancer patients as compared with Caucasians. However, recent data seem to refute ethnic difference in the types of *EGFR* mutations [12].

A predictive biomarker related to ethnic difference of sensitivity to gefitinib

Ethnic difference might also exist in sensitivity to drugs. In most such cases, gene polymorphism including microsatellite polymorphism and single nucleotide polymorphism may explain ethnic difference of response to drugs.

Using microarray technique, we analyzed gene expression profiles of peripheral mononuclear cells in lung cancer patients receiving gefitinib as a first-line monotherapy. Our results revealed that HLA genotype was closely related to response to this agent. On the other hand, large ethnic difference of HLA genotype was recognized. Previous reports have demonstrated that HLA genotype plays a role in the metabolism of certain drugs and may be a prognostic factor in malignancies such as gastric, ovarian, and cervical cancers [6, 11, 13, 15, 17]. We hypothesize that HLA subtype may be related to response to gefitinib and might explain ethnic differences. Cross-validation study of this HLA biomarker is ongoing.

Ethnic difference of gefitinib toxicity profile

Subpopulation analysis of gefitinib's toxicity in the ISEL study revealed that only southwest Asian and Taiwanese patients exhibited high ratios of interstitial lung disease (ILD) while on this therapy [16]. However, ILD might not have been induced by gefitinib. More interestingly, the data indicated that Indian–British patients experienced severe (grade 3) skin toxicity along with higher response to gefitinib. Although these phenomena are based on subpopulation analysis, we can speculate that ethnic difference might guide toxicity as well as clinical response to EGFR-TKI. Genomic and biomarker research is necessary to further elucidate these preliminary findings.

Acknowledgment We thank Dr. N. Thatcher (Christie Hosp NHS Trust) for personal communication with T. Kato.

References

1. Amador ML, Oppenheimer D, Perea S, Maitra A, Cusati G, Iacobuzio-Donahue C, Baker SD, Ashfaq R, Takimoto C, Forastiere A, Hidalgo M (2004) An epidermal growth factor receptor intron 1 polymorphism mediates response to epidermal growth factor receptor inhibitors. Cancer Res 64:9139–9143
2. Calvo E, Baselga J (2006) Ethnic differences in response to epidermal growth factor receptor tyrosine kinase inhibitors. J Clin Oncol 24:2158–2163
3. Cohen EE, Lingen MW, Martin LE, Harris PL, Brannigan BW, Haserlat SM, Okimoto RA, Sgroi DC, Dahiya S, Muir B, Clark JR, Rocco JW, Vokes EE, Haber DA, Bell DW (2005) Response of some head and neck cancers to epidermal growth factor receptor tyrosine kinase inhibitors may be linked to mutation of *ERBB2* rather than *EGFR*. Clin Cancer Res 11:8105–8108

4. Douglas DA, Zhong H, Ro JY, Oddoux C, Berger AD, Pincus MR, Satagopan JM, Gerald WL, Scher HI, Lee P, Osman I (2006) Novel mutations of epidermal growth factor receptor in localized prostate cancer. Front Biosci 11:2518–2525
5. Gwak GY, Yoon JH, Shin CM, Ahn YJ, Chung JK, Kim YA, Kim TY, Lee HS (2005) Detection of response-predicting mutations in the kinase domain of the epidermal growth factor receptor gene in cholangiocarcinomas. J Cancer Res Clin Oncol 131:649–652
6. Klein B, Klein T, Nyska A, Shapira J, Figer A, Schwartz A, Rakovsky E, Livni E, Lurie H (1991) Expression of HLA class I and class II in gastric carcinoma in relation to pathologic stage. Tumour Biol 12:68–74
7. Lee JW, Soung YH, Kim SY, Nam HK, Park WS, Nam SW, Kim MS, Sun DI, Lee YS, Jang JJ, Lee JY, Yoo NJ, Lee SH (2005) Somatic mutations of *EGFR* gene in squamous cell carcinoma of the head and neck. Clin Cancer Res 11:2879–2882
8. Lee SC, Lim SG, Soo R, Hsieh WS, Guo JY, Putti T, Tao Q, Soong R, Goh BC (2006) Lack of somatic mutations in *EGFR* tyrosine kinase domain in hepatocellular and nasopharyngeal carcinoma. Pharmacogenet Genomics 16:73–74
9. Liu W, Innocenti F, Chen P, Das S, Cook EH Jr, Ratain MJ (2003) Interethnic difference in the allelic distribution of human epidermal growth factor receptor intron 1 polymorphism. Clin Cancer Res 9:1009–1012
10. Lynch TJ, Bell DW, Sordella R, Gurubhagavatula S, Okimoto RA, Brannigan BW, Harris PL, Haserlat SM, Supko JG, Haluska FG, Louis DN, Christiani DC, Settleman J, Haber DA (2004) Activating mutations in the epidermal growth factor receptor underlying responsiveness of non-small-cell lung cancer to gefitinib. N Engl J Med 350:2129–2139
11. Ogoshi K, Tajima T, Mitomi T, Makuuchi H, Tsuji K (1997) HLA-A2 antigen status predicts metastasis and response to immunotherapy in gastric cancer. Cancer Immunol Immunother 45:53–59
12. Riely GJ, Pao W, Pham D, Li AR, Rizvi N, Venkatraman ES, Zakowski MF, Kris MG, Ladanyi M, Miller VA (2006) Clinical course of patients with non-small cell lung cancer and epidermal growth factor receptor exon 19 and exon 21 mutations treated with gefitinib or erlotinib. Clin Cancer Res 12:839–844
13. Ryu KS, Lee YS, Kim BK, Park YG, Kim YW, Hur SY, Kim TE, Kim IK, Kim JW (2001) Alterations of HLA class I and II antigen expression in preinvasive, invasive and metastatic cervical cancers. Exp Mol Med 33:136–144
14. Schilder RJ, Sill MW, Chen X, Darcy KM, Decesare SL, Lewandowski G, Lee RB, Arciero CA, Wu H, Godwin AK (2005) Phase II study of gefitinib in patients with relapsed or persistent ovarian or primary peritoneal carcinoma and evaluation of epidermal growth factor receptor mutations and immunohistochemical expression: a gynecologic oncology group study. Clin Cancer Res 11:5539–5548
15. Shen YQ, Zhang JQ, Miao FQ, Zhang JM, Jiang Q, Chen H, Shan XN, Xie W (2005) Relationship between the downregulation of HLA class I antigen and clinicopathological significance in gastric cancer. World J Gastroenterol 11:3628–3631
16. Thatcher N, Chang A, Parikh P, Rodrigues Pereira J, Ciuleanu T, von Pawel J, Thongprasert S, Tan EH, Pemberton K, Archer V, Carroll K (2005) Gefitinib plus best supportive care in previously treated patients with refractory advanced non-small-cell lung cancer: results from a randomised, placebo-controlled, multicentre study (Iressa survival evaluation in lung cancer). Lancet 366:1527–1537
17. Vitale M, Pelusi G, Taroni B, Gobbi G, Micheloni C, Rezzani R, Donato F, Wang X, Ferrone S (2005) HLA class I antigen down-regulation in primary ovary carcinoma lesions: association with disease stage. Clin Cancer Res 11:67–72

A Photon Counting Technique for Quantitatively Evaluating Progression of Peritoneal Tumor Dissemination

Kazuyoshi Yanagihara,[1] Misato Takigahira,[1] Fumitaka Takeshita,[2] Teruo Komatsu,[1] Kazuto Nishio,[3] Fumio Hasegawa,[4] and Takahiro Ochiya[2]

[1]Central Animal Laboratory, [2]Section for Studies on Metastasis, [3]Pharmacology Division, and [4]Central RI Laboratory, National Cancer Center Research Institute, Tokyo, Japan

Abstract

We recently established a mouse model of peritoneal dissemination of human gastric carcinoma, including the formation of ascites, by orthotopic transplantation of cultured gastric carcinoma cells. To clarify the processes of expansion of the tumors in this model, nude mice were sacrificed and autopsied at different points of time after the orthotopic transplantation of the cancer cells for macroscopic and histopathologic examination of the tumors. The cancer cells grew actively in the gastric submucosa and invaded the deeper layers to reach the serosal plane. The tumor cells then underwent exfoliation and became free followed by the formation of metastatic lesions initially in the greater omentum and subsequent colonization and proliferation of the tumors on the peritoneum. Although this model allowed the detection of even minute metastases, it was not satisfactory from the viewpoint of quantitative and objective evaluation. To resolve these problems, we introduced a luciferase gene into this tumor cell line with a high metastasizing potential and carried out *in vivo* photon counting analysis. This photon counting technique was found to allow objective and quantitative evaluation of the progression of peritoneal dissemination on a real-time basis. This animal metastatic model is useful for monitoring the responses of tumors to anticancer agents. (Cancer Res 2006; 66(15): 7532-9)

Introduction

Tumor dissemination and ascites are the two major features of cancerous peritonitis. Of the various manifestations of the progression of cancer affecting the i.p. organs (gastric, hepatic, ovarian, and other cancers), cancerous peritonitis is the most closely associated with poor operative results (1–6). In particular, scirrhous gastric cancer (diffusely infiltrative carcinoma or Borrmann's type IV carcinoma or the linitis plastica type) is a high-grade gastric cancer that is difficult to detect in the early stages and is often complicated by peritoneal dissemination (7–9). Although peritoneal dissemination is an important subject, very few experimental studies have been conducted to characterize its occurrence. In general, most of the experimental models of peritoneal dissemination from gastric cancer established to date have involved direct i.p. implantation of cancer cells (10–12). Although these conventional models may allow limited examination of the later stages of peritoneal dissemination, they cannot be expected to allow reasonable evaluation of its early stages. It is well known that implanting human tumor fragments and tumor cells orthotopically into the corresponding organs of nude mice results in much higher metastatic rates (13, 14). However, only one orthotopic implantation model, scirrhous carcinoma of the stomach, has been reported (15). We recently established two scirrhous gastric carcinoma-derived tumor cell lines capable of spontaneous metastasis following ectopic implantation (16). We repeated cycles of orthotopic transplantation of these tumor cell lines, collected cancer cells from the ascitic fluid formed as a result of cancerous peritonitis, and used the collected cells for further cycles of orthotopic transplantation. In this way, we isolated cell lines (44As3, 58As1, and 58As9) with high metastasizing potential and stable metastatic characteristics (17). When these cells were implanted orthotopically into the animals, bloody ascites formed within 3 to 5 weeks, resulting in the death of the animals.

As stated above, conventionally, progression of peritoneal dissemination has been analyzed by implanting cancer cells directly into the peritoneal cavity followed by sacrifice and autopsy of the animals at certain points of time after implantation and, finally, measurement of the number and weight of the tumor nodules in the sacrificed animals (18–20). Evaluation of the efficacy of anticancer agents was also hampered by this limitation (21–25). Evaluation using these methods may be affected by subjective factors and, therefore, unsatisfactory from the viewpoint of quantitative or objective evaluation. In order for our animal model of peritoneal dissemination to be applied universally as a drug evaluation system, we needed to establish a method for quantitative observation and objective evaluation of the relevant variables.

Recent progress in the optical imaging of cancers in animal models presents many potential advantages for recreating the disease process, disease detection, screening, diagnosis, drug development, and treatment evaluation. Fluorescence-based imaging (26–35) and photon counting analysis (36–43) modalities are well developed and allow specific, highly sensitive and quantitative measurements of a wide range of tumor-related variables in mice. Herein, we have shown that photon counting technique is an effective technology in living mice.

Materials and Methods

Established highly metastatic cell lines and culture. 44As3, highly peritoneal metastatic cell line, and parent HSC-44PE, human scirrhous gastric carcinoma-derived cell line, were previously reported (16, 17). When the subclones isolated by repeated s.c. injection of HSC-44PE cells were implanted orthotopically, they spread to the greater omentum, mesenterium, etc. and caused the formation of bloody ascites in a few animals (16). We repeated cycles of isolation of ascitic tumor cells and orthotopic inoculation of these cells, in turn, into animals to isolate highly metastatic

Requests for reprints: Kazuyoshi Yanagihara, Central Animal Laboratory, National Cancer Center Research Institute, 5-1-1 Tsukiji, Chuo-ku, Tokyo 104-0045, Japan. Phone: 81-3-3542-2548; Fax: 81-3-3542-2548; E-mail: kyanagih@gan2.res.ncc.go.jp.

©2006 American Association for Cancer Research.

doi:10.1158/0008-5472.CAN-05-3259

44As3 cell lines, having a strong capability of inducing the formation of ascites (17).

The cell lines were maintained in RPMI 1640 supplemented with 10% FCS (Sigma Chemical, St. Louis, MO), 100 IU/mL penicillin G sodium, and 100 mg/mL streptomycin sulfate (Immuno-Biological Laboratories, Takasaki, Japan) in a 5% CO_2 and 95% air atmosphere at 37°C (17).

***In vivo* photon counting analysis.** 44As3 and HSC-44PE cells were transfected with a complex of 4 μg pEGF-PLuc plasmid DNA (Clontech, Palo Alto, CA) and 24 μL GeneJammer reagent (Stratagene, Cloning Systems, La Jolla, CA) in accordance with the manufacturer's instructions. Stable transfectants were selected in geneticin (400 μg/mL; Invitrogen, Carlsbad, CA), and bioluminescence was used to screen transfected clones for luciferase gene expression using the IVIS system (Xenogen, Alameda, CA). Clones expressing the luciferase gene were named 44As3Luc and HSC44Luc.

Orthotopic implantation of 1×10^6 44As3Luc and HSC44Luc cells was conducted in 6-week-old female BALB/c-*nu/nu* mice (day 0) as described previously (17). *In vivo* photon counting analysis was conducted on a cryogenically cooled IVIS system using Living Image acquisition and analysis software (Xenogen) as described previously (39).

Animal protocols were approved by the committee for Ethics of Animal Experimentation and were in accordance with the Guideline for Animal Experiments in the National Cancer Center. Mice were purchased from CLEA Japan (Tokyo, Japan). The mice were maintained under specific pathogen-free conditions and provided with sterile food, water, and cages. Ambient light was controlled to provide regular cycles of 12 hours of light and 12 hours of darkness.

Therapeutic study with irinotecan (CPT-11). The experimental mice were divided into a control group that received vehicle alone (saline) and experimental groups that received i.v. inoculation of 200 mg/kg/mouse of CPT-11, a clinically active topoisomerase I inhibitor, a level that has been reported to be highly effective in tumor growth (17). On days 3, 7, and 11, tumor-bearing mice received an i.v. injection of CPT-11. The additional injection of CPT-11 was done on days 28, 31, and 35. CPT-11 was purchased from Yakult Honsha (Tokyo, Japan) and dissolved in saline before being injected.

Statistical analysis. All data were analyzed by using the unpaired *t* test and expressed as the mean ± SE. A $P < 0.05$ was considered statistically significant.

Results

Animal model of peritoneal dissemination. The highly metastatic peritoneal cell line used in this study (44As3) was isolated by repeated cycles of orthotopic implantation of HSC-44PE cells and collection of the ascitic tumor cells as described in Materials and Methods (16, 17). As shown in Table 1 and Fig. 1, the tumor formed by this cell line was characterized by a propensity for early peritoneal dissemination and was frequently associated with the formation of ascites and the animals became moribund ~35 days after implantation. On the other hand, the graft cell survival after implantation of the parent cell line (HSC-44PE) was 67% and moribund animals were not seen until ~90 days after implantation, although no ascites formation was observed.

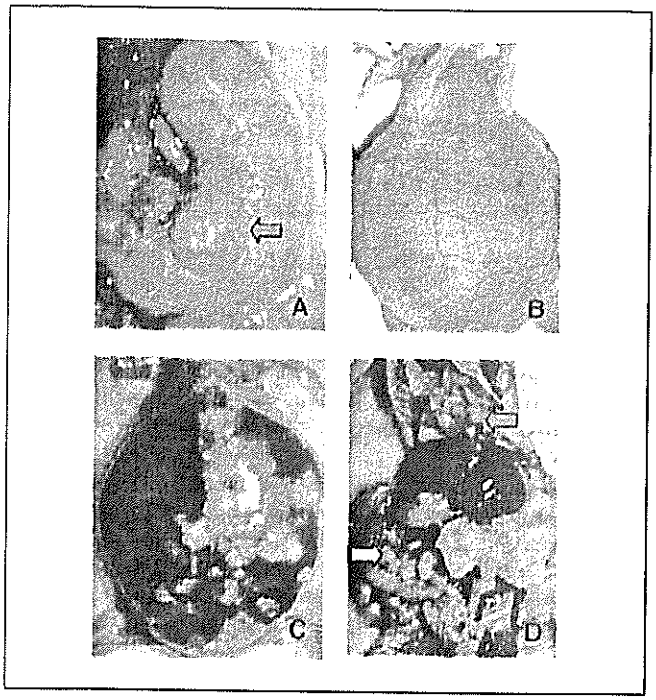

Figure 1. Macroscopic appearance of the peritoneal disseminations after orthotopic implantation of 44As3 cells. *A, green arrow,* orthotopic implantation of the cells in the stomach of nude mice was followed by tumor formation 3 weeks later. *B* and *C,* carcinomatous peritonitis was observed 5 weeks after orthotopic implantation of the cells. Abdominal distension because of bloody ascites was evident. *D,* peritoneal dissemination was recognized from the innumerable whitish nodules visualized in the abdominal cavity, mesenterium (*yellow arrow*), omentum, parietal peritoneum, and diaphragm (*green arrow*).

Anatomic, histopathologic, and ultrastructural analysis of the progression of peritoneal dissemination. To analyze the process of progression of peritoneal dissemination, 44As3 cells (1×10^6) were implanted orthotopically into the gastric wall of nude mice. Every 7 days after transplantation, five animals were

Table 1. Comparison of the survival and metastatic behavior of animals following orthotopic implantation of the highly metastatic and the parent cell lines

Cell line	Survival days	Tumor formation*	Ascites†	Disseminated metastasis				Lymph node	Liver	Pancreas‡	Kidney‡
				Omentum	Mesenterium	Peritoneum	Diaphragm				
44As3	35 ± 15 (22-65)	15/15 (100%)	14/15 (93%)	15/15	15/15	15/15	9/15	15/15	10/15	6/15	1/15
HSC-44PE	135 ± 48 (90-200)	10/15 (67%)	0/10 (0%)	5/10	3/10	3/10	0/10	5/10	0/10	0/10	0/10

*Mice were sacrificed 200 days after the orthotopic implantation. Data are the number of mice bearing metastases at the site/total number of mice bearing tumor.
†Ascites formation: >0.5 mL of ascitic fluid.
‡Micrometastases.

Table 2. Detection of metastasis and peritoneal dissemination after the orthotopic implantation of 44As3 cells

Days	Stomach	Ascites*	Disseminated metastasis				Lymph node	Liver	Pancreas†	Kidney†
			Omentum	Mesenterium	Peritoneum	Diaphragm				
7	5/5	0/5	0/5	0/5	0/5	0/5	0/5	0/5	0/5	0/5
14	5/5	0/5	3/5	0/5	0/5	0/5	1/5†	0/5	1/5	0/5
21	5/5	1/5	5/5	3/5	3/5	0/5	2/5	1/5	1/5	0/5
28	5/5	3/5	5/5	5/5	5/5	2/5	5/5	1/5	2/5	0/5
35	5/5	5/5	5/5	5/5	5/5	3/5	5/5	2/5	2/5	1/5

*Ascites formation: >0.5 mL of ascitic fluid.
†Micrometastases.

sacrificed and subjected to postmortem examination for macroscopic, histopathologic, and ultrastructural analyses (Table 2; Fig. 2). The metastatic cells (44As3) proliferated actively in the submucous tissue of the stomach (Fig. 2*A*) and began to infiltrate in the lymphatics on the 7th day. During the 2nd week following transplantation, the tumor grew more rapidly within the gastric wall, with invasion of the muscularis propria and the subserosal tissue (Fig. 2*B*). In some mice showing rapid growth of the tumor, the cancer cells broke through the serosa to become exfoliated and freed (Fig. 2*C*). These exfoliated and freed cancer cells could be visualized under the scanning electron microscope (Fig. 2*D* and *E*). Peritoneal dissemination began to be noted in the 2nd week, with cells on the greater omentum (Table 2). Micrometastases to the lymph nodes and pancreas were also noted, although not frequently. By the 3rd week, the foci of metastasis were noted in the greater omentum, mesenterium, and peritoneum. Scanning electron microscopy revealed the proliferation of the cancer cells (e.g., those colonizing the mesenterium) with the formation of larger cell clusters (data not shown). In the peritoneum, colonization of the freed cancer cells and their interaction with

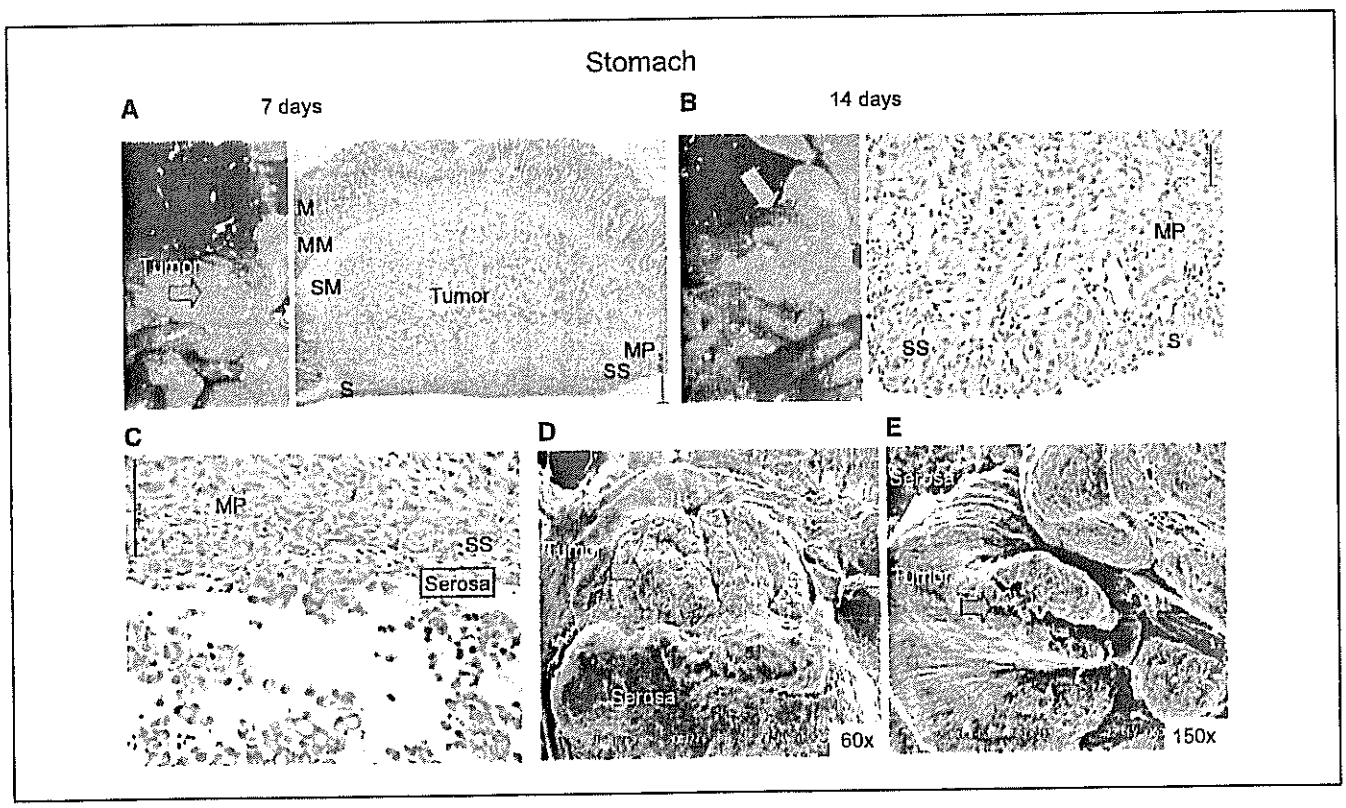

Figure 2. Macroscopic and microscopic appearance of the tumor growth of stomach of nude mice after orthotopic implantation of 44As3 cells. *A, green arrow,* orthotopic implantation of 44As3 cells in the stomach of nude mice was followed by tumor formation 7 days later. Actively proliferating 44As3 cells in the gastric submucosa (H&E). *M,* mucosa; *MM,* muscularis mucosae; *SM,* submucosa; *MP,* muscularis propria; *SS,* subserosa; *S,* serosa. *B,* tumor invasion of the muscularis propria and subserosal tissue (H&E). *C,* note 44As3 cells breaking through the serosa and becoming exfoliated and free (H&E). *D* and *E,* visualization of cancer cells breaking through the serosa and becoming exfoliated and free. Mice were sacrificed, and the tissues were examined for metastasis in various organs and processed for histologic examination as described (47, 48). Scanning electron microscopic examination was done according to standard procedures (49).

mesothelial cells were visualized (data not shown). By the 4th week, metastases to the greater omentum, mesenterium, peritoneum, and lymph nodes were noted and some animals also showed additional metastasis to the diaphragm (Table 2). Metastasis to the liver was occasionally seen. In some mice, in which the tumors grew rapidly, formation of ascites began to be noted ~21 days after the orthotopic implantation. Some of these animals became moribund on the 28th day (Tables 1 and 2). By the 35th day, all the animals showed metastasis, with dissemination to the greater omentum, mesenterium, and peritoneum accompanied by the formation of bloody ascites as well as lymph node metastasis (Table 2). Metastasis to the diaphragm was also seen frequently. Micrometastasis to the kidneys was noted in a few animals.

Analysis of the progression of dissemination using luciferase gene–tranfected cells. The analytic method described above allows detailed evaluation even of micrometastases. However, it has limitations from the viewpoint of quantitative and objective analysis. To resolve these problems, we introduced the luciferase gene into the metastatic 44As3 cell line and its parent cell line HSC-44PE by means of liposome transfer; this yielded cells with high luciferase activity, 44As3Luc and HSC44Luc, respectively. When the 44As3Luc cells (1×10^6/100 μL) were implanted s.c. into nude mice, a significant correlation was observed between tumor growth (volume) and the luciferase emission level (photon number; Fig. 3). Both cell lines were therefore used for the subsequent experiments.

The metastatic 44As3Luc or its parent cell line HSC44Luc cells were implanted orthotopically into nude mice. With the light emission noted at the site of implantation, photon counting analysis was thereafter carried out at intervals of 3 or 4 days. Figure 4*A* (*top*) presents a typical example. Chronological observation of the same animals, which were kept alive, was possible by this method. The 44As3Luc cells proliferated actively in the stomach. By the 15th day after implantation, tumor invasion of the peritoneal cavity and gradual progression of dissemination and increases in the sizes of the cell clusters were observed. Around the 25th day after implantation, a marked increase in the volume of the ascitic pool was noted by macroscopic observation, and some moribund mice were observed after the 29th day. When the moribund animals were sacrificed for autopsy, dissemination to the mesenterium and parietal peritoneum was often observed, frequently accompanied by metastasis to the lymph nodes. It was confirmed anatomically and histopathologically that the light-emitting sites corresponded to the tumor-affected sites (Fig. 4*B*). On the other hand, in the animals transplanted with the HSC44Luc, the tumor growth tended to be confined to the region of the stomach where the cells had been implanted (Fig. 4*B*), with slower tumor cell proliferation. As shown in Fig. 4*A* (*bottom*), luminescence was sometimes noted in the lymph nodes around the stomach and so on, but all of these foci of metastasis had regressed by ~60 days after implantation. Moribund animals began to be observed by the 85th day, although no ascites formation was noted in any of the animals.

By plotting the number of photons against time, a tumor growth curve reflecting the progression of peritoneal dissemination was obtained. When the relative number of photons from the highly metastatic cell line 44As3Luc and its parent cell line HSC44Luc (relative to the number of photons immediately after transplantation = 100) was plotted against time, quantitative comparison of the extents of proliferation of the two cell lines with different metastasizing potentials was possible (Fig. 4*C*).

Evaluation of the possibility of quantitative and objective screening of the effectiveness of anticancer agents. In a previous study, tumor growth was found to be suppressed in animals given i.v. injections of CPT-11, resulting in a significant prolongation

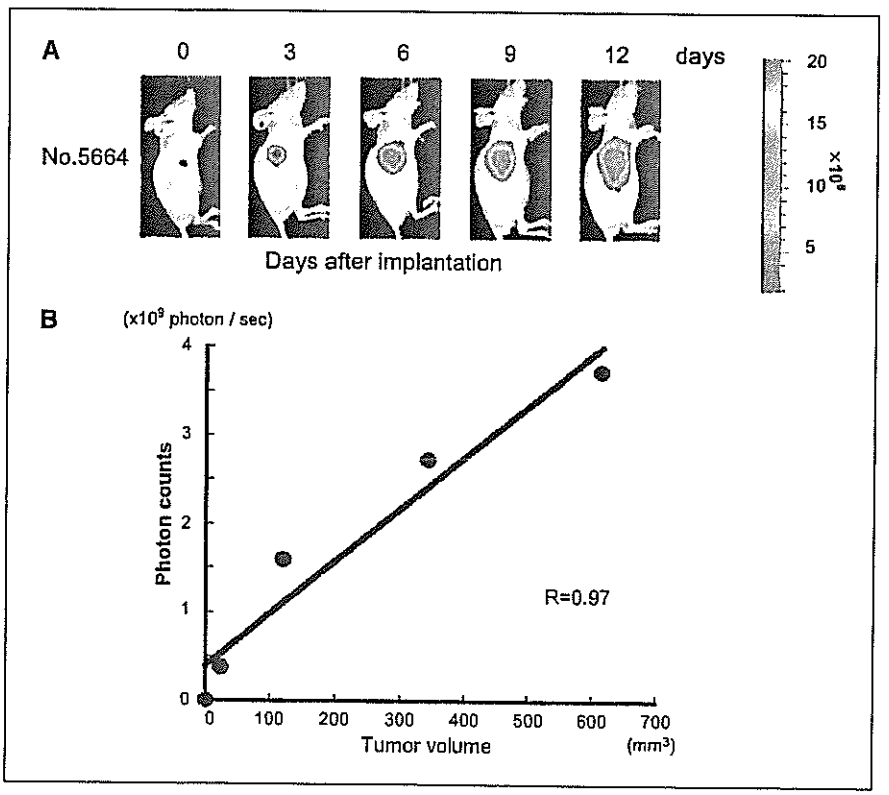

Figure 3. Correlation between the photon counts and tumor volume. *A*, nude mice bearing 44As3Luc tumors in the s.c. were visualized in anesthetized animals after i.p. inoculation of luciferin. *B*, correlation plot; strong correlation ($R = 0.97$) was observed between the conventional methods and our photon counting analysis method for monitoring the growth of a s.c. 44As3Luc tumor ($n = 5$). The tumor mass was measured at predetermined time intervals in two dimensions with calipers, and the tumor volume was calculated according to the equation $(l \times w^2) / 2$, where l is the length and w is the width (16).

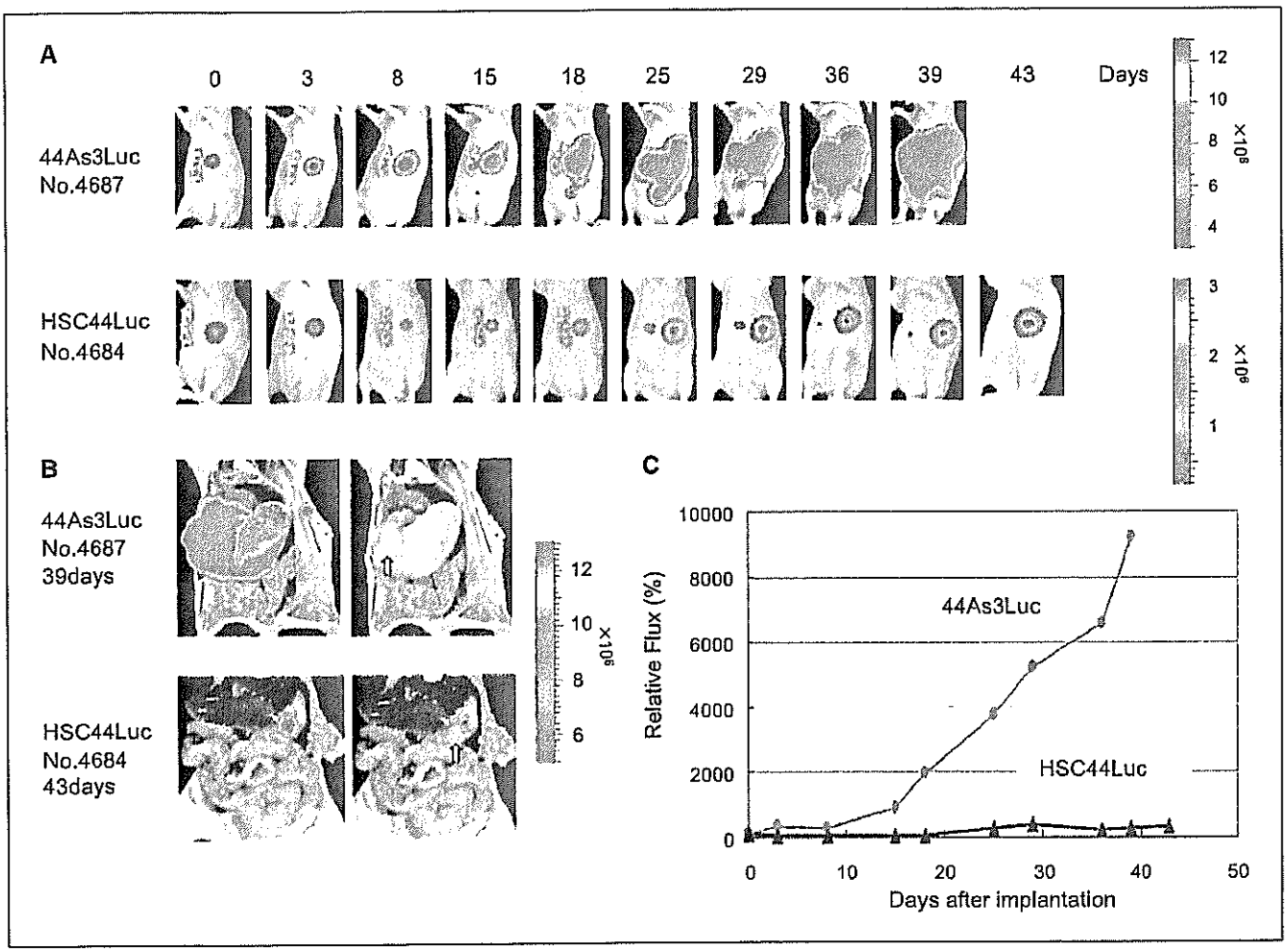

Figure 4. Quantitative photon counting analysis of progression process of peritoneal disseminated metastasis of the highly metastatic and the parent cell lines. *A*, detection of progression process of peritoneal disseminated metastasis. *B*, photon counting analysis of the peritoneal disseminations after orthotopic implantation (*yellow arrow*, site) of the cells. *C*, quantitative analysis of progression process of peritoneal disseminated metastasis of 44As3Luc (●) and HSC44Luc (▲) cell lines ($n = 5$). This experiment was repeated thrice, and similar results were observed each time.

of the survival period (17). A similar evaluation was conducted in the present study using 44As3Luc cells. Figure 5 (*top*) shows a typical example of the photon counting analysis, whereas Figure 5 (*bottom*) shows the time course of the changes in the number of photons. Following three doses of CPT-11 (200 mg/kg/mouse), the tumor gradually decreased in size, reaching a level close to the limit of detection on the 20th day. During the 5th and 6th week, the tumor began to show slow growth in the stomach followed during the 8th/9th week by peritoneal invasion and the onset of cancerous peritonitis accompanied by ascites formation and death of the animals. The survival period was markedly longer in the drug-treated group compared with that in the saline-treated controls. Plotting of the number of photons measured (average of five animals) against time yielded a tumor growth curve, thus allowing quantitative evaluation of drug-induced suppression of the progression of peritoneal dissemination (Fig. 5, *bottom*).

As stated above, the 44As3Luc cells began to proliferate again during the 5th/6th week after implantation in the CPT-11 treatment group. We therefore gave three additional doses beginning on day 28 (after the onset of reproliferation). Figure 5 (*top*) shows a typical example of the bioluminescence signal in such a case. The additional doses of CPT-11 (400 mg/kg/mouse) markedly suppressed the proliferation of the 44As3Luc cells until around day 60; however, proliferation again began to be detected thereafter. By around day 80, the tumor started to grow more rapidly and spread, causing moribund animals to appear by around day 90. The survival period of the animals was markedly prolonged by the additional drug doses. Figure 5 (*bottom*) shows the time course of changes in the number of photons (average of five animals). Quantitative comparison of the proliferation and spread of the tumor cells was possible between the drug treatment group and the control group and between two drug treatment groups, thus allowing objective evaluation of the responses to treatment.

Discussion

Before the present study, very little was known about how scirrhous gastric carcinoma cells invaded and proliferated within the primary lesion, how they exfoliated and thus became free, how they colonized and proliferated within the peritoneal cavity, or how they advanced to the stage of cancerous peritonitis. Herein, we investigated the course of proliferation and spread of gastric cancer

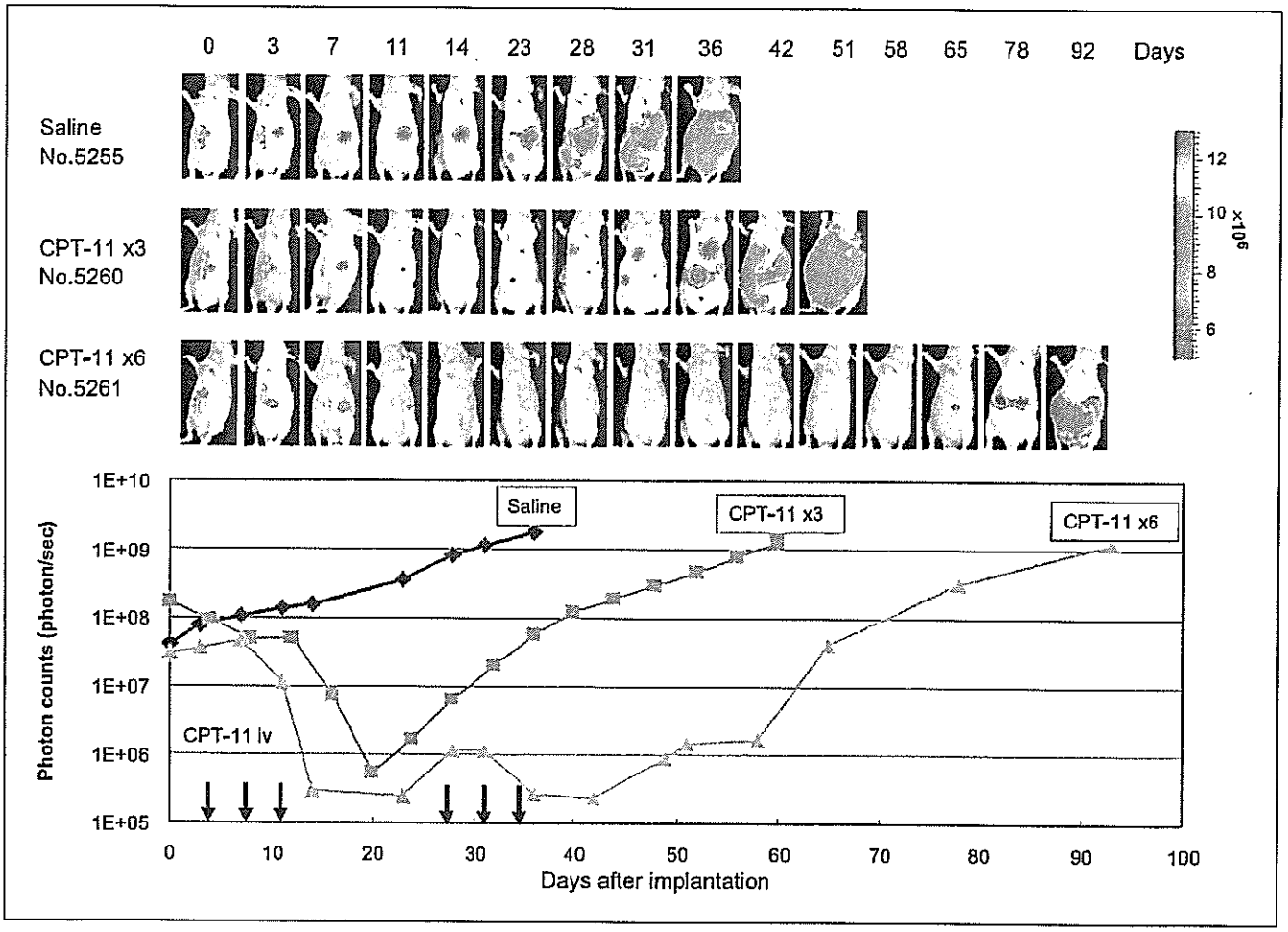

Figure 5. Quantitative photon counting analysis of the effect of CPT-11 on peritoneal disseminated metastasis 44As3Luc mouse model. Effects of CPT-11 in the peritoneal dissemination mouse model established using orthotopically implanted 44As3Luc cells. Mice receiving CPT-11 (*arrow*) or vehicle alone as control ($n = 5$; $P < 0.001$) were monitored twice weekly for the development of peritoneal dissemination. Similar results were obtained in a second experiment conducted independently.

cells by sacrificing the animals at different points of time after orthotopic implantation of the highly metastatic tumor cell line 44As3 (17) and conducted anatomic and histopathologic examinations in the sacrificed animals. In this experiment, the sequence of findings seems to endorse the previous contention that gastric cancer cells invade deeper layers of the gastric wall to reach the serosa and then exfoliate, thereby being released into the peritoneal cavity, resulting in peritoneal dissemination.

The growth of tumors in the gastric wall and the subsequent progression to cancerous peritonitis are difficult to monitor extracorporeally unlike s.c. tumors. For monitoring the progression of tumor dissemination, the only possible method was to implant the tumor cells into groups of mice and sacrifice the animals at different points of time for autopsy and observation; quantitative comparison was still not possible by this method (10–12, 18–25). All of these problems were resolved in the present study by introduction of the luciferase gene into tumor cells with a high metastasizing potential and subsequent *in vivo* photon counting analysis. In the first step, we confirmed that the results of the conventional method of evaluation in relation to proliferation of our gastric carcinoma cells were consistent with the results of our photon counting analysis. We then conducted an experiment on a model of peritoneal dissemination. Using the *in vivo* photon counting technique, it was possible to observe the same animals successively, beginning from the growth of the tumor at the site of implantation to peritoneal dissemination and, finally, the formation of ascites. Furthermore, it was possible to observe the processes of dissemination progression on a real-time basis, allowing quantitative analysis and comparison of the course of proliferation and progression within the living body after implantation of a cell line with high metastasizing potential and its parent cell line based on changes in the photon number.

Needless to say, it is important to develop a screening model for exploring substances effective against tumors and ultimately developing clinically useful anticancer agents. We previously reported that an animal model of peritoneal dissemination established using the highly metastatic cell lines (44As3, 58As1, and 58As9) established by our group satisfied all of the requirements of a model for drug screening (17, 44). However, before this model can be applied as a universally valid drug evaluation system, the following problems must be resolved: (*a*) methods for appropriate observation and objective evaluation are urgently needed,

(*b*) excellent operative skill is indispensable for orthotopic implantation with high reproducibility, and (*c*) large numbers of animals are needed. With the establishment of this experimental system, the conventional problems associated with the evaluation of peritoneal dissemination have been overcome and highly reliable data are now obtainable. Therefore, a stage has been reached where this model of peritoneal dissemination can also be applied as a system for evaluation of the effects of drugs. Furthermore, because photon counting analysis allows noninvasive evaluation of the fate of cancer cells *in vivo* on a real-time basis, the pain experienced by experimental animals may be reduced, such that this technique would also be useful from the viewpoint of animal welfare (45).

We have used the bioluminescence signal from the luciferase reporter gene in our peritoneal metastasis model. Luciferase genes in our tumor cells can function stably over significant periods in tumors and in their metastases. To date, several other peritoneal metastasis models of human stomach cancer in animals have been reported (28, 31). For example, Hasegawa et al. (28) used green fluorescent protein (GFP) retroviral-infected human stomach cancer. In this nude mouse model, tumor cells were peritoneally injected and GFP transduction allowed visualization of the subsequent metastatic process. A major advantage of GFP labeling is that imaging requires no preparative procedures and hence allows for direct visualization in living tissue (26, 27, 29, 32, 34). In contrast, photon counting technique requires exogenous injection of luciferin substrate, which can stress the animals, and in addition, the intensity of the luciferase signal may sometimes be variable and unstable (46). Furthermore, Ray et al. (32) reported that red fluorescent protein imaging is ~1,000 times stronger than that of luciferase *in vivo*. Therefore, for monitoring the tumor metastasis process at the single-cell level, fluorescence imaging may be the more practical method. In fact, fluorescence-based orthotopic metastatic models have been used to study mechanisms and for drug discovery (14, 30, 33, 35).

In conclusion, our photon counting analysis involving a highly metastatic cell line, 44As3Luc, seems to be a useful model for studies, such as those designed to clarify the mechanism of peritoneal dissemination progression in intractable scirrhous gastric carcinoma, and for the development of new agents effective against such tumors.

Acknowledgments

Received 9/22/2005; revised 3/23/2006; accepted 5/26/2006.

Grant support: Ministry of Health, Labor, and Welfare of Japan Grant-in-Aid for Cancer Research.

The costs of publication of this article were defrayed in part by the payment of page charges. This article must therefore be hereby marked *advertisement* in accordance with 18 U.S.C. Section 1734 solely to indicate this fact.

We thank Dr. A. Ochiai (Pathology Division, Research Center for Innovative Oncology, National Cancer Center at Kashiwa, Kashiwa, Japan) for helpful discussions, Dr. S. Hirohashi for generous help, and M. Kodama for excellent technical work.

References

1. Chu ZD, Lang NP, Thompson C, et al. Peritoneal carcinomatosis in nongynecological malignancy. A prospective study of prognostic factors. Cancer 1989; 63:364–7.
2. Moriguchi S, Maehara Y, Korenaga D, et al. Risk factors which predict pattern of recurrence after curative surgery for patients with advanced gastric cancer. Surg Oncol 1992;1:341–6.
3. Averbach AM, Jacquet P. Strategies to decrease the incidence of intra-abdominal recurrence in resectable gastric cancer. Br J Surg 1996;83:726–33.
4. Tanahashi H, Konishi M, Nakagohri T, et al. Aggressive multimodal treatment for peritoneal dissemination and needle tract implantation of hepatocellular carcinoma: a case report. Jpn J Clin Oncol 2004;34:551–5.
5. Heintz AP. Surgery in advanced ovarian carcinoma: is there proof to show the benefit? Eur J Surg Oncol 1988; 14:91–9.
6. Hoskins WJ. Prospective on ovarian cancer: why prevent? J Cell Biochem Suppl 1995;23:189–99.
7. Kaibara N, Iitsuka Y, Kimura A, et al. Relationship between area of serosal invasion and prognosis in patients with gastric carcinoma. Cancer 1987;60:136–9.
8. Hamazoe R, Maeta M, Kaibara N. Intraperitoneal thermochemotherapy for prevention of peritoneal recurrence of gastric cancer. Final results of a randomized controlled study. Cancer 1994;73:2048–52.
9. Katano M, Morisaki T. The past, the present, and future of the OK-432 therapy for patients with malignant effusions. Anticancer Res 1998;18:3917–25.
10. Kotanagi H, Saito Y, Shinozawa N, Koyama K. Establishment of a human cancer cell line with high potential for peritoneal dissemination. J Gastroenterol 1995;30:437–8.
11. Kaneko K, Yano M, Tsujinaka T, et al. Establishment of a visible peritoneal micrometastatic model from a gastric adenocarcinoma cell line by green fluorescent protein. Int J Oncol 2000;16:893–8.
12. Nomura H, Nishimori H, Yasoshima T, et al. A novel experimental mouse model of peritoneal dissemination of human gastric cancer cells: analysis of the mechanism of peritoneal dissemination using cDNA macroarrays. Jpn J Cancer Res 2001;92:748–54.
13. Furukawa T, Fu X, Kubota T, et al. Nude mouse metastatic models of human stomach cancer constructed using orthotopic implantation of histologically intact tissue. Cancer Res 1993;53:1204–8.
14. Hoffman RM. Orthotopic metastatic mouse models for anticancer drug discovery and evaluation: a bridge to the clinic. Invest New Drugs 1999;17:343–59.
15. Yashiro M, Chung YS, Nishimura S, et al. Peritoneal metastatic model for human scirrhous gastric carcinoma in nude mice. Clin Exp Metastasis 1996;14:43–54.
16. Yanagihara K, Tanaka H, Takigahira M, et al. Establishment of two cell lines from human gastric scirrhous carcinoma that possess the potential to metastasize spontaneously in nude mice. Cancer Sci 2004;95:575–82.
17. Yanagihara K, Takigahira M, Tanaka H, et al. Development and biological analysis of peritoneal metastasis mouse models for human scirrhous stomach cancer. Cancer Sci 2005;96:323–32.
18. Fujita S, Suzuki H, Kinoshita M, Hirohashi S. Inhibition of cell attachment, invasion, and metastasis of human carcinoma cells by anti-integrin β_1 subunit antibody. Jpn J Cancer Res 1992;83:1317–26.
19. Nakashio T, Narita T, Akiyama S, et al. Adhesion molecules and TGF-β1 are involved in the peritoneal dissemination of NUGC-4 human gastric cancer cells. Int J Cancer 1997;70:612–8.
20. Ishii Y, Ochiai A, Yamada T, et al. Integrin $\alpha_6\beta_4$ as a suppressor and a predictive marker for peritoneal dissemination in human gastric cancer. Gastroenterology 2000;118:497–506.
21. Nishimura S, Adachi M, Ishida T, et al. Adenovirus-mediated transfection of caspase-8 augments anoikis and inhibits peritoneal dissemination of human gastric carcinoma cells. Cancer Res 2001;61:7009–14.
22. Minagawa A, Otani Y, Kubota T, et al. The citrus flavonoid, nobiletin, inhibits peritoneal dissemination of human gastric carcinoma in SCID mice. Jpn J Cancer Res 2001;92:1322–8.
23. Kimata M, Otani Y, Kubota T, et al. Matrix metalloproteinase inhibitor, marimastat, decreases peritoneal spread of gastric carcinoma in nude mice. Jpn J Cancer Res 2002;93:834–41.
24. Piso P, Aselmann H, von Wasielewski R, et al. Prevention of peritoneal carcinomatosis from human gastric cancer cells by adjuvant-type intraperitoneal immunotherapy in a SCID mouse model. Eur Surg Res 2003;35:470–6.
25. Yonemura Y, Endou Y, Bando E, et al. Effect of intraperitoneal administration of docetaxel on peritoneal dissemination of gastric cancer. Cancer Lett 2004; 210:189–96.
26. Chishima T, Miyagi Y, Wang X, et al. Cancer invasion and micrometastasis visualized in live tissue by green fluorescent protein expression. Cancer Res 1997;57: 2042–7.
27. Hoffman RM. The multiple uses of fluorescent proteins to visualize cancer *in vivo*. Nat Rev Cancer 2005;5:796–806.
28. Hasegawa S, Yang M, Chishima T, et al. *In vivo* tumor delivery of the green fluorescent protein gene to report future occurrence of metastasis. Cancer Gene Ther 2000; 7:1336–40.
29. Bouvet M, Wang J, Nardin SR, et al. Real-time optical imaging of primary tumor growth and multiple metastatic events in a pancreatic cancer orthotopic model. Cancer Res 2002;62:1534–40.
30. Sun F-X, Tohgo A, Bouvet M, et al. Efficacy of camptothecin analog DX-8951f (Exatecan Mesylate) on human pancreatic cancer in an orthotopic metastatic model. Cancer Res 2003;63:80–5.
31. Nakanishi H, Mochizuki Y, Kodera Y, et al. Chemosensitivity of peritoneal micrometastases as evaluated using a green fluorescence protein (GFP)-tagged human gastric cancer cell line. Cancer Sci 2003;94:112–8.
32. Ray P, De A, Min JJ, et al. Imaging tri-fusion multimodality reporter gene expression in living subjects. Cancer Res 2004;64:1323–30.
33. Hoffman RM. Orthotopic metastatic (MetaMouse) models for discovery and development of novel chemotherapy. Methods Mol Med 2005;111:297–322.

34. Nakanishi H, Ito S, Mochizuki Y, Tatematsu M. Evaluation of chemosensitivity of micrometastases with green fluorescent protein gene-tagged tumor models in mice. Methods Mol Med 2005;111:351–62.
35. Hennig R, Ventura J, Segersvard R, et al. LY293111 improves efficacy of gemcitabine therapy on pancreatic cancer in a fluorescent orthotopic model in athymic mice. Neoplasia 2005;7:417–25.
36. Contag PR, Olomu IN, Stevenson DK, Contag CH. Bioluminescent indicators in living mammals. Nat Med 1998;4:245–7.
37. Rehemtulla A, Stegman LD, Cardozo SJ, et al. Rapid and quantitative assessment of cancer treatment response using *in vivo* bioluminescence imaging. Neoplasia 2000;2:491–5.
38. Jenkins DE, Oei Y, Hornig YS, et al. Bioluminescent imaging (BLI) to improve and refine traditional murine models of tumor growth and metastasis. Clin Exp Metastasis 2003;20:733–44.
39. Vooijs M, Jonkers J, Lyons S, Berns A. Noninvasive imaging of spontaneous retinoblastoma pathway-dependent tumors in mice. Cancer Res 2002;62:1862–7.
40. Takeshita F, Minakuchi Y, Nagahara S, et al. Efficient delivery of small interfering RNA to bone-metastatic tumors by using atelocollagen *in vivo*. Proc Natl Acad Sci USA 2005;102:12177–82.
41. Lyons SK. Advances in imaging mouse tumour models *in vivo*. J Pathol 2005;205:194–205.
42. Hiraga T, Williams PJ, Ueda A, et al. Zoledronic acid inhibits visceral metastases in the 4T1/luc mouse breast cancer model. Clin Cancer Res 2004;10:4559–67.
43. Laurie NA, Gray JK, Zhang J, et al. Topotecan combination chemotherapy in two new rodent models of retinoblastoma. Clin Cancer Res 2005;11:7569–78.
44. Arao T, Yanagihara K, Takigahira M, et al. ZD6474 inhibits tumor growth and intraperitoneal dissemination in a highly metastatic orthotopic gastric cancer model. Int J Cancer 2006;118:483–9.
45. El Hilali N, Rubio N, Martinez-Villacampa M, Blanco J. Combined noninvasive imaging and luminometric quantification of luciferase-labeled human prostate tumors and metastases. Lab Invest 2002;82:1563–71.
46. Burgos JS, Rosol M, Moats RA, et al. Time course of bioluminescent signal in orthotopic and heterotopic brain tumors in nude mice. Biotechniques 2003;34:1184–8.
47. Yanagihara K, Seyama T, Tsumuraya M, et al. Establishment and characterization of human signet ring cell gastric carcinoma cell lines with amplification of the c-*myc* oncogene. Cancer Res 1991;51:381–6.
48. Yanagihara K, Kajitani T, Kamiya K, Yokoro K. *In vitro* studies on the mechanism of leukemogenesis-I. Establishment and characterization of cell lines derived from the thymic epithelial reticulum cell of the mouse. Leuk Res 1981;5:321–9.
49. Domagala W, Koss LG. Surface configuration of mesothelial cells in effusions. A comparative light microscopic and scanning electron microscopic study. Virchows Arch B Cell Pathol Incl Mol Pathol 1979;30:231–43.

Breast Cancer Research and Treatment (2006) 99: 9–17
DOI 10.1007/s10549-006-9175-2

© Springer 2006

Gene expression profiling of ATP-binding cassette (ABC) transporters as a predictor of the pathologic response to neoadjuvant chemotherapy in breast cancer patients

Sarah Park[1,5], Chikako Shimizu[2], Tatsu Shimoyama[1], Masayuki Takeda[1], Masashi Ando[2], Tsutomu Kohno[2], Noriyuki Katsumata[2], Yoon-Koo Kang[5], Kazuto Nishio[1,3,4], and Yasuhiro Fujiwara[2]

[1]*Shien Lab, National Cancer Center Hospital, Tokyo, Japan;* [2]*Breast and Medical Oncology, National Cancer Center Hospital, Tokyo, Japan;* [3]*Pharmacology Division, National Cancer Center Research Institute, Tokyo, Japan;* [4]*Center for Medical Genomics, National Cancer Center Research Institute, Tokyo, Japan;* [5]*Division of Hematology Oncology, Asan Medical center, University of Ulsan College of Medicine, Seoul, Korea*

Key words: ATP-binding-cassette (ABC) transporters, breast cancer, class prediction, neoadjuvant chemotherapy, oligonucleotide microarray

Summary

Drug resistance is a major obstacle to the successful chemotherapy. Several ATP-binding cassette (ABC) transporters including ABCB1, ABCC1 and ABCG2 have been known to be important mediators of chemoresistance. Using oligonucleotide microarrays (HG-U133 Plus 2.0; Affymetrix), we analyzed the ABC transporter gene expression profiles in breast cancer patients who underwent sequential weekly paclitaxel/FEC (5-fluorouracil, epirubicin and cyclophosphamide) neoadjuvant chemotherapy. We compared the ABC transporter expression profile between two classes of pretreatment tumor samples divided by the patients' pathological response to neoadjuvant chemotherapy (residual disease [RD] versus pathologic complete response [pCR]) ABCB3, ABCC7 and ABCF2 showed significantly high expression in the pCR. Several ABC transporters including ABCC5, ABCA12, ABCA1 ABCC13, ABCB6 and ABCC11 showed significantly increased expression in the RD ($p<0.05$). We evaluated the feasibility of developing a multigene predictor model of pathologic response to neoadjuvant chemotherapy using gene expression profiles of ABC transporters. The prediction error was evaluated by leave-one-out cross-validation (LOOCV). A multigene predictor model with the ABC transporters differentially expressed between the two classes ($p \leq 0.003$) showed an average 92.8% of predictive accuracy (95% CI, 88.0–97.4%) with a 93.2% (95% CI, 85.2–100%) positive predictive value for pCR, a 93.6% (95% CI, 87.8–99.4%) negative predictive value, a sensitivity of 88.1%(95% CI, 76.8–99.4%), and a specificity of 95.9% (91.1% CI, 87.8–100%). Our results suggest that several ABC transporters in human breast cancer cells may affect the clinical response to neoadjuvant chemotherapy, and transcriptional profiling of these genes may be useful to predict the pathologic response to sequential weekly paclitaxel/FEC in breast cancer patients.

Introduction

Resistance to chemotherapy is a significant obstacle to appropriate treatment of cancer patients. Various cellular pathways may play a role in drug resistance and ATP-binding cassette (ABC) transporters are one of the most well known mediators leading to drug resistance and treatment failure. To date 49 ABC transporter genes have been identified and classified into seven groups, ABCA, ABCB, ABCC, ABCD, ABCE, ABCF, and ABCG (database of ABC transporters available at http://nutrigene.4t.com/humanabc.htm).

Extensive studies have been conducted on the individual proteins or genes of ABC transporter members regarding their role in chemoresistance. ABCB1 (MDR1-P-gp) [1,2], ABCC1 (MRP1) [3], and ABCG2 (MXR) [4] are particularly well known as mediators leading to resistance to several chemotherapeutic agents including paclitaxel [5], topoisomerase inhibitors [6], anthracyclin [7] and tyrosine kinase inhibitors [8]. Although little has been known about most of ABC transporter members, other members of this family sharing sequence and structural homology may play roles in absorption, distribution, and excretion of chemotherapeutic agents and probably influence the response to chemotherapy.

Recently, using ABC transporter gene expression profiling, studies on the relationship of drug resistance and ABC transporter were performed in cancer cell lines [9,10].

The characterization of the comprehensive expression of these genes in relation to the clinical response to chemotherapy may be useful to determine on an individual basis the patient's underlying risk and choose the optimal therapeutic regimen to which the individual cancer patient is most likely to respond. We studied the relationship between ABC transporter gene expression and the responsiveness to chemotherapy in early breast cancer patients who underwent sequential weekly paclitaxel/FEC (5-fluorouracil, epirubicin and cyclophosphamide) neoadjuvant chemotherapy and evaluated the feasibility of developing a multigene predictor model of pathologic response using differentially expressed ABC transporters on the basis of microarray data.

Materials and methods

Patient and sample preparation

This study was performed at the National Cancer Center Hospital, Tokyo, Japan. This study was approved by the institutional review boards of the National Cancer Center. Twenty-one pretreatment samples were obtained from breast cancer patients who underwent neoadjuvant chemotherapy from 2002 to 2004. All patients underwent pretreatment core needle biopsy (CNB) of the primary tumor tissue before starting neoadjuvant chemotherapy. The core needle biopsy was done using 14–16 gauge needles.

The patients received 4 cycles of FEC (5-Fluorouracil 500 mg/m^2, Epirubicin 100 mg/m^2 and Cyclophosphamide 500 mg/m^2) every three weeks followed by 12 cycles of weekly paclitaxel (80 mg/m^2). Additionally, in the case of HER2 positive determined by immunohistochemical staining (IHC), the specific inhibitory antibody of HER2 receptor, Trastuzumab (Herceptin®) was added in the course of the paclitaxel (Herceptin 4 mg/kg on day1 then 2 mg/kg weekly). Samples that showed 3 + IHC staining were considered as HER2 positive.

Every patient underwent surgery on the completion of the neoadjuvant chemotherapy, and histopathologic examination was performed. As described previously [11], pathologic complete response (pCR) was defined as no pathologic evidence of any residual invasive cancer cells in the breast and axillary lymph nodes, and residual disease (RD) was defined as any residual cancer cells on the histopathologic examination. Informed consent was obtained from all patients for voluntary participation in the study.

Tissue preparation and microarray

Samples for the microarray were collected into tubes containing Isogen (Nippon gene, Toyama) and stored at −80 °C. Total RNA was extracted by the single step method of Chomczynski et al. [12] with acid guanidinium thiocyanate phenol chloroform after homogenizing the tissue using a high speed homogenizer. The mean yield of RNA was 23.1 μg (ranged from 12.3 to 31.6 μg) from each collected samples. RNA that had distinct ribosomal RNA band by electrophoresis and had A_{260}/A_{280} absorbance ratio ranging from 1.8 to 2.1 was used for cDNA synthesis. Gene expression profiles were analyzed on a high-density oligonucleotide microarray (GeneChip® HG-U133 Plus 2.0; Affymetrix, Santa Clara, CA) containing 54,675 probe sets. The oligonucleotide microarray procedure for generation of the biotin-labeled cyclic RNA (cRNA) by *in vitro* transcription, hybridization to the array and scanning were performed according to the manufacturer's instructions. The amplification cycle of RNA to cDNA and cDNA to cRNA was performed using the GeneChip® 3′-Amplification Reagents One-Cycle cDNA Synthesis Kit including SuperScript II reverse transcriptase and a T7-$(dT)_{24}$ primer (Affymetrix). The synthesized cRNA was biotinylated using GeneChip 3′-amplification reagents for IVT labeling. The labeled cRNA was then purified and chemically fragmented at 94 °C for 35 min using the GeneChip Sample Cleanup Module (Affymetrix). The labeled fragmented cRNA was next hybridized to the GeneChip® at 45 °C for 16 h according to the manufacturer's instructions. The hybridized probe array was washed and stained with streptavidin-phycoerythrin. The stained probe array was scanned with a GeneChip® Scanner3000 (Affymetrix) at 570 nm. The signal intensity of the gene expression level was calculated by GeneChip Operating Software, Ver.1 (Affymetrix).

Data analysis

Microarray data analyses were performed with BRB ArrayTools developed by Dr. Richard Simon and Amy Peng Lam. (http://linus.nci.nih.gov/BRB-ArrayTools.html) which provides a variety of tools for the analysis of gene expression profile. Gene expression data were log transformed (base 2) and normalized to the median expression value of all genes on each array. Any genes in which the expression levels did not differ by at least by 1.5 fold from the median in at least 20% of the arrays were filtered out, for the exclusion of the genes showing minimal variation across the set of arrays. In addition, if an expression value was missing or filtered out in more than 50%, these data were excluded. The final data set included 50,508 clones, and contained all 49 ABC transporter genes. The list of transcripts on ABC transporters was obtained using GeneSprings software (http://www.silicongenetics.com/cgi/SiG.cgi/index.smf) from Agilent Technologies (Waldbronn, Germany). (Supplementary data).

Class comparison

To identify informative genes differentially expressed between the two classes of patients grouped by their pathologic response, we used supervised classification methods applying the random variance *t*-test to data using the BRB Array Tools and was accompanied by multivariate permutation tests in order to minimize false-positives with the maximum allowed number of

false positives set at 10, a false discovery rate of 0.1, and confidence 90%. Genes with a parametric p-value less than 0.05 were considered statistically significant.

Class prediction

To develop a prediction model of pathologic response using the ABC transporter gene expression profiles, we used the class prediction tools of BRB ArrayTools in which six multivariate classification methods were available including a compound covariate predictor [13], a K-nearest neighbor analysis ($K=1, 3$), a nearest centroid analysis, a support vector machine [14] and a diagonal linear discriminate analysis.

For the evaluation of the feasibility of developing a multigene predictor model of response to neoadjuvant chemotherapy using differentially expressed ABC transporters, six different multivariate classification models were examined. Firstly, we determined the number of genes that were included in the classifier model using a paired t-test applying multiple univariate parametric significance thresholds, and developed a classifier model based on these selected genes at the univariate parametric significance thresholds. With changes in the parametric significance thresholds, the multivariate classification algorithms were performed iteratively evaluating the classification error and the classifier p-value to identify the best classifier, and the processes were iteratively performed for each number of genes included in the classifier (determined by the significance threshold). The prediction error of each model was evaluated by leave-one-out cross-validation (LOOCV) [15]. This validation procedure was performed in a manner that removed the left-out sample before selecting the discriminate genes [15,16]. The classifier p-value, the probability that similar low error rate happen by chance, was obtained by a random permutation test performed 2000 times.

Results

The patient characteristics

All the patients received 4 courses of FEC (5-fluorouracil, epirubicin and cyclophosphamide) combination chemotherapy followed by 12 courses of weekly paclitaxel. In those patients who were HER-2 positive by IHC, Trastuzumab (Herceptin®) was added in the course of the treatment. We divided the patients into two groups from the results of the histopathologic examination performed after the completion of the neoadjuvant chemotherapy. Pathologic data were available for nineteen patients. Patients with no pathologic evidence of any residual invasive cancer cells in breast were classified as 'pCR', and if any residual cancer cells were found in the histopathologic study, these patients were classified as 'RD' group. Thirty-six point eight percent (7) of the nineteen patients showed no pathologic evidence of any residual invasive cancer cells in the breast and were classified as pCR and 63.2% (12) of patients were classified as RD.

Gene expression profiling of differentially expressed ABC transporters

Using gene expression data of the pretreatment tumor sample, we compared the ABC transporter gene expression profile between the two groups (RD versus pCR). A probe set on all of the 49 human ABC transporters genes known so far was contained in the microarray chip we used (HG-U133 Plus 2.0; Affymetrix). To identify differentially expressed ABC transporter genes potentially associated with the clinical response to neoadjuvant chemotherapy, a supervised class comparison analysis was performed. The random variance model t-test was used to discover differentially expressed genes and was accompanied by a multivariate 1000 permutation tests in order to minimize false-positives with the maximum allowed number of false positives set at 10, a false discovery rate of 0.1 and 90% confidence.

By comparing the average expression level of each transcript on ABC transporters between the two classes of patients, the median expression level in the RD group was 107.8 (range 15.8–6009.1) and 104.4 in the pCR group (range 17.9–5690.6). The median of fold difference (RD: pCR) of transcripts on the ABC transporters was 1.0, ranging from 0.3 to 7.6. Several ABC transporters showed prominently high expression at over 50 fold of the median value although the tumor samples were all from the pretreatment chemotherapy-naïve patients. The highest average expression level in the RD group, 6009.1, was observed in ABCC5 (AF146074, RD: pCR=6009.1:2427.5, fold ratio 2.48) and the highest expression level in the pCR group, 5690.6, was observed in TAP1 (ABCB2, NM_000593, RD: pCR = 4551.4:5690.6, fold ratio 0.8), the transporter associated with antigen processing (Table 1).

The ABC transporters, which were significantly differentially expressed with a parametric p-value of less than 0.05, are listed in Table 2. Several transcripts (ABCC5, TAP2/ABCB3) selected overlapped for the microarray chip (HG-U133 Plus 2.0) containing 54,675 probe sets, more than 30,000 human transcripts were detected, derived from more than 20,000 loci within the human genome and some transcripts represented the same human gene.

ABC transporters, the expression of which in the RD group was significantly increased, included ABCC5 (fold ratio 2.48, $p=0.000368$), ABCA12 (fold ratio 7.64, $p=0.000795$), ABCA1 (fold ratio 3.30, $p=0.000859$), ABCC13 (fold ratio 7.54, $p=0.0194$), ABCB6 (fold ratio 2.17, $p=0.0271$), and ABCC11 (fold ratio 2.71, $p=0.0486$) (Table 2). These genes all showed over 2 fold increases in RD compared with pCR tumors. ABCC5 was recently reported to confer resistance to

Table 1. Clinical characteristics of the patients

	No. of patients
Age, years	
Median	51
Range	30-61
Menstruation status	
Pre menopause	12
Post menopause	7
TNM stage	
IIA	8
IIB	7
IIIA	2
IIIB	2
Histology	
Invasive ductal	17
Mixed ductal/lobular	
Invasive lobular	1
Invasive mucinous	1
Nuclear grade	
1	1
2	9
3	9
HER2 status	
HER2-positive	4
HER2-negative	15
ER status	
ER-positive*	5
ER-negative	14
Pathologic response	
Pathologic complete response	7
Residual disease	12
Treatment arm	
A[a]	15
B[b]	4

*Cases in which more than 10% of tumor cells stained positive for ER by IHC classified as ER positive.
[a]Treatment arm A; 4 courses of FEC* followed by 12 courses of weekly paclitaxel.
[b]Treatment arm B; 4 courses of FEC* followed by 12 courses of weekly paclitaxel with Trastuzumab.
*FEC combination chemotherapy (5-fluorouracil, epirubicin and cyclophosphamide).

5-fluorouracil [17] selected with the lowest p-value and it showed the highest gene expression level in tumors with decreased response. (AF146074, expression level RD: pCR = 6009.1: 2427.5, fold ratio 2.48).

CFTR (NM_000492, ABCC7, fold ratio 0.27, p = 0.007030), ABCF2 (NM_005692, fold ratio 0.32, p = 0.015901) and ABCB3 (M74447, TAP2, fold ratio 0.54, p = 0.019345), the transporter associated with antigen processing, showed increased expression in the pCR group but the biological significance concerning responsiveness to chemotherapy remains to be elucidated. The differentially expressed ABC transporter genes are shown in Figure 1 in hierarchical clustering view.

Development of multigene predictor model using the ABC transporter gene expression profile

To evaluate the feasibility of developing a multigene predictor model of response to neoadjuvant chemotherapy using the ABC transporter expression profile, six different multivariate classification models were examined.

Firstly, we determined the number of discriminate genes that were included in the classifier model by applying multiple univariate parametric significance thresholds, and developed a classifier model based on these selected genes at the significance thresholds. With changes in the parametric significance thresholds, the classification error and classifier p-value for each multivariate classification algorithms were evaluated iteratively by LOOCV (leave one out cross validation) [15] and the random permutation test to identify the best classifier model. The classifier p-value, the probability that a similar low error rate could happen by chance, was calculated by 2000 random permutation tests. We calculated the average of the classification error and the classifier p-value of six classifier models at each significance threshold. Figure 2 shows the change in the average classifier p-value for six multivariate classification models from the permutation test and the average of the classification error rate relative to multiple univariate parametric significance thresholds.

During this iterative process, the average estimated misclassification error and classifier p-value also dropped as the significance threshold decreased to 0.003, but applying further stringent significance thresholds caused a steep increase in the classification error. When the ABC transporters differentially expressed between the two classes at a significance threshold level of 0.003 were used for class prediction, the average of the classification error was minimal, 0.072 (92.8% of predictive accuracy, 95% CI, 88.0–97.4%), with the classifier p = 0.012, 93.2% (95% CI, 85.2–100%) positive predictive value for the pCR group, 93.6% (95% CI, 87.8–99.4%) negative predictive value, sensitivity for the pCR group 88.1% (95% CI, 76.8–99.4%), and a specificity of 95.9% (91.1% CI, 87.8–100%). The respective values for each model are represented in Table 3. On applying the compound covariate predictor classifier model, the predictive accuracy reached 100% with a classifier p-value of 0.0005. The ABC transporters selected as the best classifiers are presented in Table 4. The list included ABCA1, ABCA12 and ABCC5, recently reported to confer resistance to cyclic nucleotides including 5-fluorouracil [17].

Our results suggest that the ABC transporter genes expression pattern may be useful in predicting the pathologic response to sequential weekly paclitaxel/FEC in breast cancer patients.

Discussion

To determine the optimal therapeutic regimen to which the individual cancer patient is most likely to respond on